Ultrahigh-throughput–directed enzyme evolution by absorbance-activated droplet sorting (AADS)

Fabrice Gielen[a,1], Raphaelle Hours[a,1], Stephane Emond[a], Martin Fischlechner[a,b], Ursula Schell[c], and Florian Hollfelder[a,2]

[a]Department of Biochemistry, University of Cambridge, Cambridge, CB2 1GA, United Kingdom; [b]Institute for Life Sciences, University of Southampton, Southampton, SO17 1BJ, United Kingdom; and [c]Johnson Matthey Plc, Cambridge, CB4 0WE, United Kingdom

Edited by Frances H. Arnold, California Institute of Technology, Pasadena, CA, and approved October 12, 2016 (received for review May 20, 2016)

Ultrahigh-throughput screening, in which members of enzyme libraries compartmentalized in water-in-oil emulsion droplets are assayed, has emerged as a powerful format for directed evolution and functional metagenomics but is currently limited to fluorescence readouts. Here we describe a highly efficient microfluidic absorbance-activated droplet sorter (AADS) that extends the range of assays amenable to this approach. Using this module, microdroplets can be sorted based on absorbance readout at rates of up to 300 droplets per second (i.e., >1 million droplets per hour). To validate this device, we implemented a miniaturized coupled assay for NAD^+-dependent amino acid dehydrogenases. The detection limit (10 μM in a coupled assay producing a formazan dye) enables accurate kinetic readouts sensitive enough to detect a minimum of 1,300 turnovers per enzyme molecule, expressed in a single cell, and released by lysis within a droplet. Sorting experiments showed that the AADS successfully enriched active variants up to 2,800-fold from an overwhelming majority of inactive ones at ∼100 Hz. To demonstrate the utility of this module for protein engineering, two rounds of directed evolution were performed to improve the activity of phenylalanine dehydrogenase toward its native substrate. Fourteen hits showed increased activity (improved >4.5-fold in lysate; k_{cat} increased >2.7-fold), soluble protein expression levels (up 60%), and thermostability (T_m, 12 °C higher). The AADS module makes the most widely used optical detection format amenable to screens of unprecedented size, paving the way for the implementation of chromogenic assays in droplet microfluidics workflows.

protein engineering | directed evolution | microfluidics | ultrahigh-throughput | emulsion droplets

Directed evolution has arguably become the most popular method to generate enzymes with improved and altered activities (1–5), but the success of this approach is dependent on exploring a maximum of combinatorial diversity (6). Therefore, screening of large libraries of variants is essential and technologies to trawl sequence space efficiently are required. Massive scale-down of assay volumes by compartmentalization of library members in water-in-oil emulsion droplets has recently led to the development of ultrahigh-throughput screening platforms that use small volumes (typically picoliters) and allow sorting of more than 10^6 variants per hour (7–9) (cf., schematic in Fig. 1*A*). The key technical module to make this possible is a microfluidic droplet sorter that has so far relied exclusively on fluorescent readouts (fluorescence-activated droplet sorting, FADS) (10, 11). By alternatively transforming microfluidic emulsions to double emulsions (12) or hydrogel beads equipped with polyelectrolyte shells (13), sorting in standard flow cytometers also becomes possible. However, to date, all ultrahigh-throughput screening campaigns implemented in microcompartmentalized formats (including microcapillary arrays) have so far relied on detection of a fluorescent product (13–20). When assays that lack this type of readout are to be used (e.g., involving instead the widely used absorbance detection), droplet screening is currently impossible: Colony screening assays (relying on precipitation of insoluble product and thus encumbered by poor dynamic range and assay quality) or microwell-plate screening with sophisticated robots (higher quality but expensive in terms of capital expenditure and running costs) remain the only options. In the present work, we remedy this unsatisfactory situation and report a microfluidic absorbance detection module suitable for ultrahigh-throughput microdroplet sorting that was validated by successful enzyme evolution. The target chemistry chosen is the NAD^+-dependent deamination of amino acids catalyzed by phenylalanine dehydrogenase (PheDH), a representative of the large class of oxidoreductases (21, 22). Variants of PheDH are selected by absorbance-activated droplet sorting (AADS), based on the ability of our device to deliver high levels of enrichment (∼2,800-fold).

Results

Design of a Microfluidic Sorter Based on Absorbance Detection. The conversion of L-phenylalanine (L-Phe) to phenyl pyruvate by PheDH was detected in a coupled reaction, in which the oxidation of NADH leads to the coupled reduction of a water-soluble tetrazolium salt, WST-1, to give a formazan dye (in the presence of the electron coupling reagent mPMS; Fig. 1*B*). To detect the formazan product, an absorbance setup was designed, in which two optical fibers—aligned face-to-face across the droplet channel (Fig. 2*A*)—were embedded into a planar microfluidic chip (*SI Appendix*, Fig. S1 *A* and *B*). Whenever a droplet passes through the interrogation volume, a decrease in transmittance relative to its dye concentration is recorded and used as the basis of a sorting decision. To detect small transmittance changes, the power of the LED light source was maximized so that the photodiode detector worked close to its saturation level and the estimated detection limit for WST-1 formazan was ∼7.5 μM

Significance

Directed enzyme evolution is a powerful approach for discovering new catalysts with applications in green chemistry and elsewhere. However, "hits" in sequence space are rare: If too few members of a library are examined, the chances of success of a campaign are limited. Ultrahigh-throughput screening in emulsion droplets has dramatically increased the odds but requires a fluorescent reaction product that triggers selection of hits. We now introduce an absorbance-based microfluidic droplet sorter that broadens the scope of assays to those producing UV/Vis-active chromophores and demonstrate its usefulness by evolving a dehydrogenase based on the screening of half a million library members. Making ultrahigh-throughput screening possible for previously inaccessible reactions enables much wider use of microfluidic droplet sorters for laboratory evolution.

Author contributions: F.G., U.S., and F.H. designed research; F.G., R.H., and S.E. performed research; F.G. and M.F. contributed new reagents/analytic tools; F.G., R.H., S.E., and F.H. analyzed data; and F.G., R.H., S.E., M.F., and F.H. wrote the paper.

Conflict of interest statement: U.S. is an employee of Johnson Matthey. R.H. is the recipient of an Engineering and Physical Sciences Research Council (EPSRC) Collaborative Awards in Science and Engineering (CASE) studentship jointly funded by Johnson Matthey and the EPSRC.

This article is a PNAS Direct Submission.

[1]F.G. and R.H. contributed equally to this work.

[2]To whom correspondence should be addressed. Email: fh111@cam.ac.uk.

This article contains supporting information online at www.pnas.org/lookup/suppl/doi:10.1073/pnas.1606927113/-/DCSupplemental.

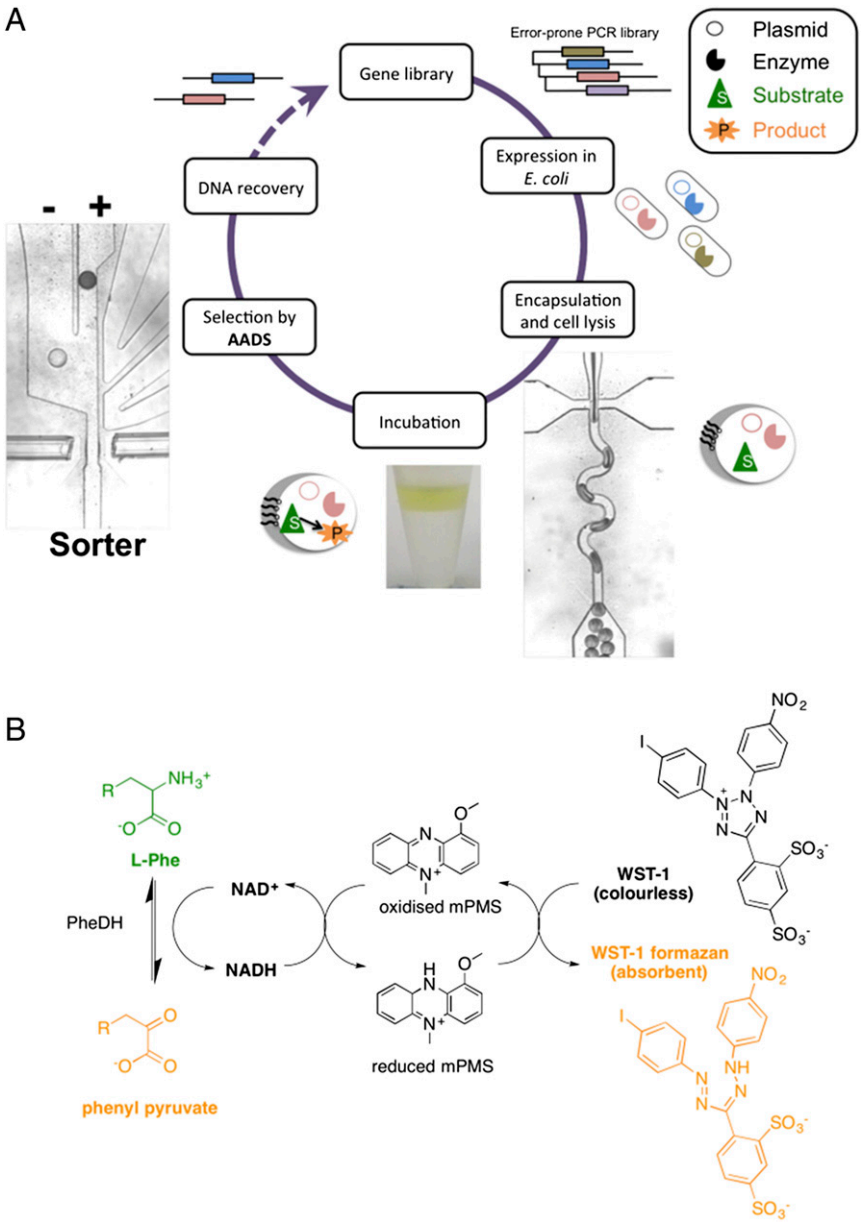

Fig. 1. Directed evolution cycle based on sorting of microdroplets by their absorbance. (*A*) Droplets are generated to encapsulate single cells together with a lysis agent and substrates, incubated in tubing, and reinjected into the sorting module. This AADS module relies on head-on fiber optics embedded in the microdroplet sorting device that are used to measure on-the-fly transmittance as droplets pass in-between the fibers. (*B*) Scheme for the reaction of the NAD^+-dependent PheDH from Rhodococcus sp. M4 (PheDH). The reduction of the cofactor NAD^+ to NADH in the deamination direction is detected by a coupled assay involving the electron coupling reagent 1-methoxy-5-methylphenazinium methyl sulfate (mPMS) and the reduction of the water-soluble tetrazolium salt 2-(4-iodophenyl)-3-(4-nitrophenyl)-5-(2,4-disulfophenyl)-2H-tetrazolium (WST-1) to give the absorbing dye WST-1 formazan.

(*SI Appendix*, *A.1*). We experimentally verified the sensitivity of the setup by measuring dilutions of the dye. Readouts from the photodetector for droplets with increasing concentrations of WST-1 formazan from 0 to 4 mM are shown in Fig. 2*B* (larger plots are available in *SI Appendix*, Fig. S2). The transmittance was calculated from the average voltage corresponding to the center of the droplets, away from the signal spikes originating from refraction at the oil–water interface of droplets crossing the detection chamber. Although the transmittance values for droplets decrease with increasing WST-1 formazan, the signal for the oil remains constant. In practice, the droplet transmittance is greater than that of the oil at low WST-1 formazan concentration and less than that of the oil at high concentrations (*SI Appendix*, Fig. S3). From these data, an absorbance calibration plot was constructed (Fig. 2*C*), showing excellent linearity over a wide range of concentrations (based on monitoring >200 droplets, with low coefficients of variation <5%). The sensitivity depends on good fiber alignment minimizing stray light, which, in our case, was measured to be <0.5% (determined with a strongly absorbing food dye). The experimental limit of detection (Fig. 2) was thus found to be around 10 μM WST-1 formazan, nearly coinciding with the previous estimate and suggesting that the device is optimally implemented.

Operation and Calibration of the Absorbance Sorter. During AADS screening campaigns, improved enzyme variants producing more absorbing product than the wild-type catalyst have to be detected and sorted by activation of on-chip electrodes that pull droplets

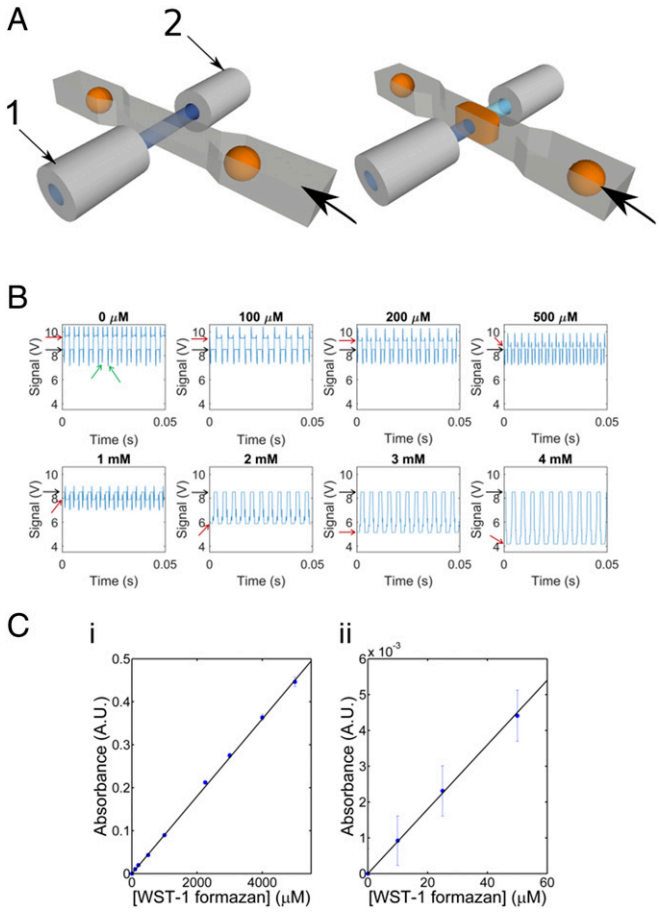

Fig. 2. AADS for droplet microfluidics. (*A*) Schematic of the head-on fiber optics on both sides of a microchannel. One fiber (*1*) is coupled to a light source, whereas the one facing it across the droplet channel (*2*) is coupled to a photodetector. When a droplet passes through the interrogation volume, the intensity of light detected decreases concomitantly with its concentration of a chromogenic dye. (*B*) Dilution series for the detection of WST-1 formazan. Series of droplets read in sequence for several concentrations (here covering a range from 0 to 4 mM WST-1). The scatter signal at the edges of droplets (marked by green arrows) defines the boundaries of an absorbance measurement in one droplet. The transmittance value for each droplet is read as the average value in-between these edges. The relative positions of the transmittance values for the droplet content and the oil phase (indicated as red vs. black arrows on the left) cross over around 650 μM WST-1 formazan (see *SI Appendix*, Fig. S2 for larger versions of the plots shown here), because the droplet signal is greater than the invariant baseline signal for the oil below this concentration and less than that above. For the sorting of libraries, 1 mM WST-1 formazan was added to minimize the signal spikes caused by scattering at droplet boundaries at low dye concentrations: For [WST-1 formazan] >2 mM, the spikes all but disappear. (*C*) Calibration plot showing the linearity of absorbance across a range of WST-1 formazan concentrations using the readout shown in *A*, in two different concentration regimes: (*i*) between 0 and 5 mM and (*ii*) from 0 to 50 μM (glycine–KOH buffer, 100 mM, pH 10, 20 °C).

toward the sorting channel dielectrophoretically (11, 23). To validate the microfluidic operation of the sorter, mixtures of droplets containing (*i*) PBS buffer or, alternatively, (*ii*) dilutions of a strongly absorbing black food dye were generated, stored in tubing, and reinjected into the sorting chip. An open-source Arduino board (Arduino Due) was used to monitor the voltage signal of the detector in real time and to compare this voltage to a threshold value below which a trigger was released (*SI Appendix*, *A.5*). This trigger signal, in turn, activated the high-voltage AC field applied to the electrodes (*SI Appendix*, Fig. S4 *A* and *B*). Snapshots of a droplet in the process of being sorted (recognizable by the encapsulated black dye) are displayed in Fig. 3*A* (see Movie S1).

The maximum droplet frequency at which stable and reliable sorting was achieved depended on the total flow rate (the sum of oil and emulsion flow rates): The faster the droplets moved through the sorting junction, the higher the electric field required for sorting had to be (Fig. 3*B*). Spacing oil was injected fast enough to bring about a large separation between droplets within the channel and ensure single droplet sorting (*SI Appendix*, *A.2*). With a square wave of 3 ms (1,000 V_{pp}, 10 kHz), a sorting frequency of over 300 Hz (at a total flow rate of 80 μL/min) could be achieved with droplets of 70 μm in diameter.

The current sorting algorithm simply compares real-time analog voltage to an arbitrary user-set voltage threshold. That implies that low dye concentrations (<100 μM) cannot be sorted, because they are effectively masked by signal spikes induced by refractive index mismatch between the phases (carrier oil, $n = 1.29$; dispersed aqueous phase, $n = 1.34$; see Fig. 2*B* and *SI Appendix*, Fig. S5 and *A.4*). To bypass this limitation, an offset of 1 mM WST-1 formazan was added in the single-cell sorting experiments to enable sorting

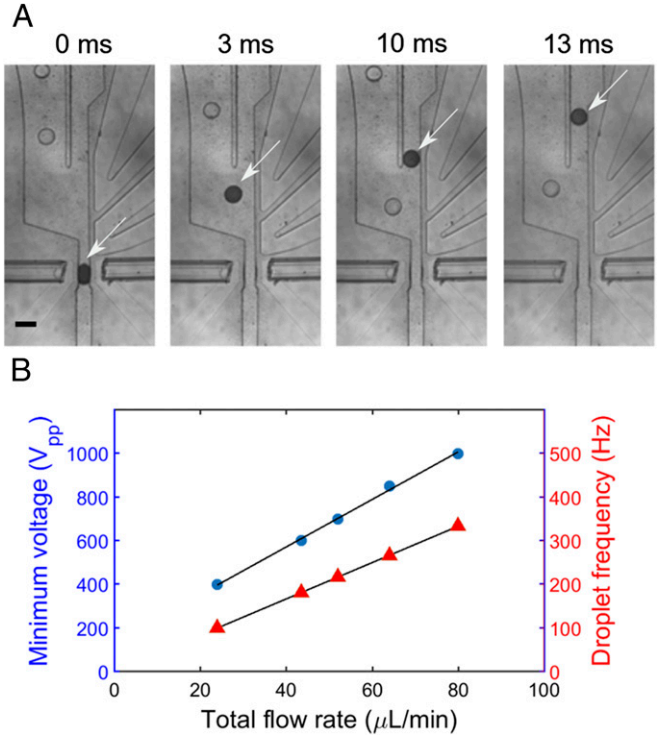

Fig. 3. Operation of AADS. (*A*) Snapshots of microdroplets selectively directed toward the sorting channel by triggering embedded electrodes on their absorbance signal. The white arrows on each snapshot track a droplet as it is being pushed toward the sorting channel. Optical fibers were inserted into guide microchannels and adjusted to be in close proximity (~50 μm) to the droplet channel. A narrower neck (width, 50 μm; channel height, 80 μm) induces local elongation of the droplet, which facilitates absorbance measurements. The flow pattern in the device was designed so that droplets would naturally flow to the waste channel (*Left*) in the absence of an electric field. Whenever a transmittance below a set voltage threshold was detected, electric pulses (square 1 kV_{pp}, 10 kHz, ~5 ms long) were applied to attract droplets dielectrophoretically toward the sorting channel (*Right*). Salt water electrodes were used to conduct the electric field. (Scale bar, 125 μm.) (*B*) Calibration of the voltage (blue) required for successful sorting of droplets and the corresponding droplet sorting frequency (red) as a function of total flow rate (spacing oil plus emulsion). The ratio of the flow rate of emulsion to the spacing carrier phase was typically kept constant (1:15). Black lines are linear fits drawn to guide the eye.

with better sensitivity by masking the spikes (~10 μM WST-1 formazan; see Fig. 2*B*).

Time Courses of Product Formation from Single-Cell Picoliter Lysates. The required incubation time for single-cell lysate assays is dependent on the activity of the enzyme but also crucially on the droplet volume, because the amount of enzyme cannot exceed the quantity expressed by a single cell. To determine the incubation time necessary to detect product formation, time courses of the reaction with wild-type PheDH (wtPheDH) were performed. To this end, ~10^5 cells expressing wtPheDH were encapsulated into ~10^6 single emulsion droplets to ensure single-cell occupancy according to Poisson statistics, along with substrate L-Phe (10 mM; i.e., > K_M, to test under conditions of maximal turnover rate) and lysis agents. The droplet absorbance was subsequently measured in the sorter at different incubation times to monitor the progress of the reaction (Fig. 4*A* and *SI Appendix*, Fig. S6).

Importantly, droplet-to-droplet cross-contamination of the reaction product was not observed (24), as droplets adjacent to positive droplets did not show detectable intake of dye over the course of the experiment (5 h; see *SI Appendix*, *A.3*). The signal reached saturation after 2 h of incubation, resulting in 2 mM WST-1 formazan production from a starting concentration of 10 mM L-Phe, indicating either depletion of or inhibition by at least one of the components within the droplets or enzyme inactivation.

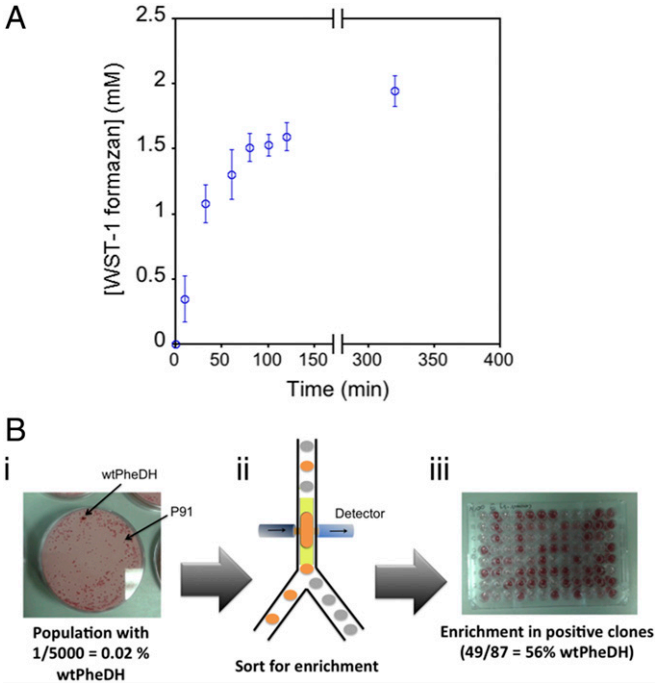

Fig. 4. Detection and sorting of PheDH activity based on absorbance in droplets. (*A*) Time-dependent single-cell lysate in droplets for the reaction of wtPheDH. Conditions: [L-Phe], 10 mM; [NAD^+], 10 mM; [WST-1], 5 mM; [mPMS], 5 μg/mL; in glycine–KOH buffer (100 mM), pH 10, 25 °C. Incubation time for library screening was chosen in order for wtPheDH to be close to the assay end point (>2 h). (*B*) Enrichment of cells by AADS based on PheDH activity. (*i*) *E. coli* cells expressing either wtPheDH or an enzyme not active on L-Phe (P91) were mixed at a 1:5,000 ratio before compartmentalization into single droplets; this population was analyzed by colony screening to detect PheDH activity (showing here the detection of one active colony out of ~5,000 screened in total). (*ii*) After compartmentalization, droplets were sorted after 3 h of reaction (~2 mM WST-1 formazan) to enrich for cells expressing wtPheDH. (*iii*) The sorted population was analyzed for PheDH activity by microplate cell lysate assays to determine enrichment ratios [here, 49 colonies (56%) were active out of 87 screened in total, corresponding to an enrichment value of 2,800].

Given the enzyme's catalytic efficiency (k_{cat}/K_M ~7×10^4 $M^{-1}{\cdot}s^{-1}$; *SI Appendix*, Table S2) and the observation of ~10^6 active enzymes produced per cell (*SI Appendix*, *Text B*, Table S1, and Fig. S14), the lower detection limit of the sorter (10 μM WST-1 formazan in a 180 pL droplet) is surpassed after 60 s, from which point onwards the reaction can be monitored and its signal used for sorting.

Sorting Efficiency Quantified by Enrichment Analysis. The ability to isolate droplets containing an active enzyme that produces an absorbing downstream product (e.g., WST-1 formazan) was tested first by mimicking a library sorting experiment to enrich droplets containing wtPheDH from an overwhelming majority of droplets containing an enzyme not active on L-Phe (the phosphotriesterase P91) (15). After expression of both enzymes in separate liquid cultures, around 10^5 cells were mixed in a 1:5,000 ratio before Poisson-distributed single-cell compartmentalization with 10 mM substrate (i.e., L-Phe). After collection in a syringe and incubation (3 h), the droplets were injected into the absorbance sorting chip, and the ones containing active PheDH were collected based on WST-1 formazan product absorbance. After sorting, the plasmid DNA was recovered from droplets and transformed into *Escherichia coli* cells, which were subsequently grown on agar plates overnight. To estimate the enrichment ratio (defined as the percentage of positive variants after sorting divided by the same percentage before sorting), randomly picked colonies were screened for PheDH activity (Fig. 4*B*). The experiment yielded a 2,800-fold enrichment, corresponding to 56% positive hits in the sorted population. As previously shown (10), enrichment is mainly limited by accidental coencapsulation of negative and positive variants. Additional false-positives specific to absorbance detection include the presence of light-absorbing objects (e.g., dust particles, precipitates) inside droplets or the measurement of two droplets in close contact creating an enhanced scatter at their interface (see examples in Movie S2). In a typical model-sorting experiment, false-positive rates were found to be below 5% of sorted events. To further control the process, videos of sorting events were continuously and automatically acquired (via camera software) and saved, so that successful sorting could be ensured by inspection of videos during and after the experiment (see Movie S3 for examples of 10 short clips).

Directed Evolution of wtPheDH. Next, the activity of wtPheDH toward its native substrate L-Phe was increased by directed evolution to further test whether the workflow outlined in Fig. 1*A* can yield improved enzymes. An error-prone PCR library of wtPheDH (**Lib0**; 10^6 transformants, 1.7 mutations per gene) was constructed and transformed into *E. coli*. Before sorting, randomly picked library members were assayed for cell lysate activity against L-Phe in 96-well plates to establish the activity profile of **Lib0**. This preliminary analysis (Fig. 5*A*) showed that the majority of variants (>90%; *SI Appendix*, Fig. S9) were highly deleterious (i.e., showing >twofold decreased activity relative to wtPheDH), whereas positive variants (showing >1.3-fold improvement relative to wtPheDH; i.e., significantly more than the SD) were less abundant (<1%; *SI Appendix*, Fig. S9). To enrich positive variants while maintaining high screening throughput, this library was sorted in droplets using a 1:2 (cell:droplet) ratio (forfeiting single-cell occupancy according to Poisson statistics for higher throughput). Around 5×10^5 cells (each of them expressing a single PheDH variant) were compartmentalized into single emulsions, along with 10 mM substrate. After incubation for 3 h at room temperature, these droplets were injected into the AADS device and sorted at ~100 Hz with a selection threshold set to collect the 0.2% most absorbing droplets (*SI Appendix*, Fig. S8). This yielded ~1,000 selected variants after DNA recovery and retransformation. Analysis of this sorted population in microwell plates (Fig. 5*A*) showed that

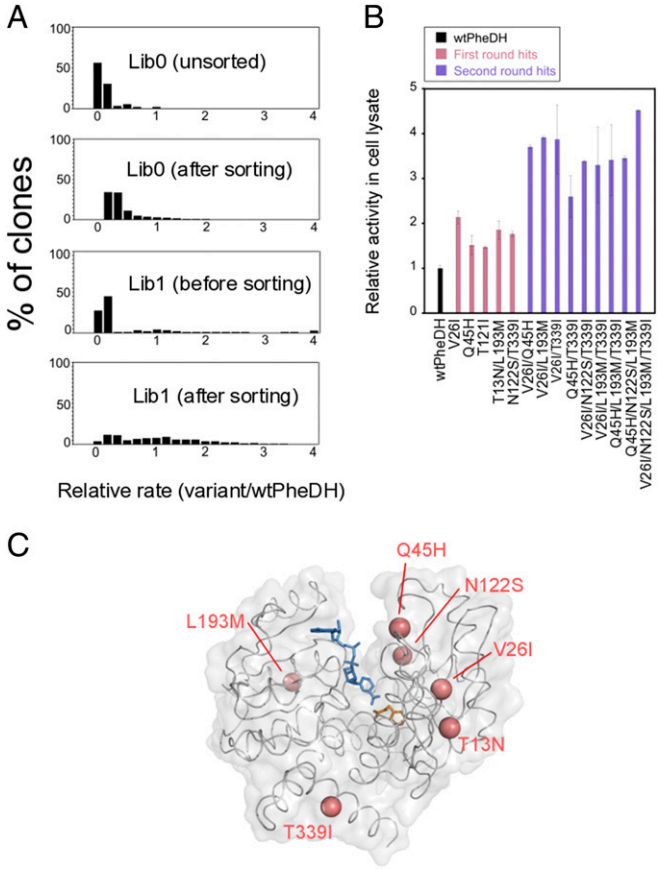

Fig. 5. Directed evolution of wtPheDH for increased activity against L-Phe. (*A*) Enrichment of positive hits over two rounds of droplet sorting. Shown are relative rates of 96 variants that were randomly picked from the original library (Lib0) and after each round of sorting (Lib0–Lib1). The data were normalized to the rate of wtPheDH (=1). (*B*) Activity changes among selected variants from the first and the second round of evolution. The activity for each variant is plotted relative to that of wtPheDH. Data are averages of triplicate values from three independent experiments, and error bars represent ±1 SEM. (*C*) The structure of wtPheDH (Protein Data Bank ID code 1BW9) with residues that were mutated in the two rounds of evolution shown in pink. The active site contains phenyl pyruvate (orange) and NAD^+ (blue).

the sorting experiment successfully enriched positives (~6% of the sorted population; *SI Appendix*, Fig. S9) by at least sixfold, along with a decrease in the proportion of deleterious mutants (from >90% to 75%; *SI Appendix*, Fig. S9). Five mutants (containing mutations T13N, V26I, Q45H, T121I, N122S, L193M, and T339I; Fig. 5*C*) with up to 2.2-fold improved relative activity in cell lysates were identified (Fig. 5*B*), of which three showed improved soluble expression of the enzyme (up to twofold compared with wtPheDH; *SI Appendix*, Fig. S11). These results demonstrate that screening a higher number of variants under high droplet occupancy [e.g., using a 1:2 (cell:droplet) ratio] is an effective strategy to enrich a population for rare positive variants (e.g., from <1% before sorting to ~6% after) that conventional plate screening approaches are unlikely to recover because of limited throughput (see *SI Appendix*, Fig. S9). For the second round of evolution, a shuffling library (**Lib1**; 10^6 transformants) was generated to identify beneficial combinations of the first-round hit mutations. As in the first round, the PheDH activity profile of the library was analyzed before screening by AADS (Fig. 5*A* and *SI Appendix*, Fig. S10). Around 10% of the assayed variants showed >twofold increased activity relative to wtPheDH (*SI Appendix*, Fig. S10). To enrich the library population for these potential hits, around 10^5 cells were compartimentalized into 10^6 single emulsions [i.e., corresponding to a 1:10 (cell:droplet) ratio for further AADS under single-cell occupancy conditions]. The selection threshold was set to collect the 1% most absorbing droplets (corresponding to the 10% most active variants; Fig. 5*A* and *SI Appendix*, Fig. S8), finally yielding ~800 variants after DNA recovery and retransformation. The top 5% of the variants (with ≥ threefold improvements) were sequenced, leading to the identification of nine additional hits combining two to four mutations (Fig. 5*B*). Among these, the quadruple mutant V26I/N122S/L193M/T339I showed the highest improvement under our screening conditions, with a 4.6-fold improvement in lysate activity (relative to that of wtPheDH) (Fig. 5*B*). The k_{cat} measured with purified protein was 2.7-fold improved (*SI Appendix*, Fig. S12 and Table S2), whereas no improvement in k_{cat}/K_M was observed, because K_M and k_{cat} showed compensatory behavior (*SI Appendix*, Table S2). Instead, this variant showed a 2.2-fold increase in soluble expression indicative of improved folding efficiency (*SI Appendix*, Fig. S11) as well as increased thermostability (T_m value increased by ~12 °C at pH 8) and a half-life of inactivation at 50 °C increased by 7.5-fold (*SI Appendix*, Fig. S13 and Tables S3 and S4). Overall, this directed evolution experiment yielded 14 improved variants, demonstrating the validity of our approach. In single-cell lysate assays, the readout is a combination of the enzyme's activity, solubility, stability, and its amount expressed within the cell, which is reflected in the enhanced properties of the selected enzyme variants. The mutations identified mainly affected solvent-exposed residues (V26I, Q45H, L193M, T339I; Fig. 5*C*), which may be indicative of their involvement in protein stabilization and folding efficiency (25–27). One mutation (N122S) is located close to the catalytic residue D118, in a region previously shown to be involved in substrate specificity in amino acid dehydrogenases (28).

Discussion

A Sensitive Sorting Device Based on Absorbance Readouts. The limited sensitivity of absorbance detection when working with small path lengths has generally been seen to preclude its use as a quantitative readout for droplet microfluidics assays. The design feature that makes our sorter useful for single-cell selections is the relatively large droplet volume (180 pL; diameter, 70 μm) that boosts sensitivity (by a larger path length) while keeping the sample/volume ratio high (1 million compartments generated from only 180 μL). This high sample/volume ratio and a screening rate of ~300 per second exceed the throughput of assays in multiwell plates by 1,000-fold (14). In addition, building the system is relatively straightforward: Fiber-coupled LED sources and standard SI-photodiode detectors are inexpensive, integration of optical fibers on chip bypasses the need for optical tables and alignment procedures, and microcontroller actuation of the sorter is simple to implement (see *SI Appendix*, Fig. S4*B*). Further important design features of the microfluidic sorter are (*i*) the proximity of the detection area and the sorting junction (within 400 μm) to synchronize detection and sorting events; (*ii*) the slight squeezing of droplets in the detection area to form plugs that separate edge spikes from assay absorbance, ensuring reproducible measurements; (*iii*) the alignment of the detection point with the sorting channel to maximize the dielectrophoretic force acting on the droplets; and (*iv*) the use of a pressure equilibrator before the outlets to minimize hydrostatic effects on droplet flow, as reported previously (29). Previous absorbance measurements in droplets have lower analytical throughput [<10 Hz in published work (30–34); i.e., an order of magnitude below AADS] and crucially lack the connection to a sorting module, preventing their use for directed evolution.

Absorbance assays are intrinsically 3–4 orders of magnitude less sensitive compared with fluorescence assays: In platforms such as FACS or FADS, concentrations as low as 2.5 nM fluorescein can be readily detected (15, 18). Nevertheless, the ability to quantify

micromolar concentrations of absorbing reaction product (~10 μM) will make many established enzymatic assays accessible for droplet-based ultrahigh-throughput screening. The performance of AADS could be further improved by using monochromatic laser light with a wavelength centered at the absorption maximum of the dye, embedding optical cavities on chip, which can increase sensitivity about fivefold (35), or using a lock-in amplifier to extract the signal from electronic noise (36). Further increases in the sorting frequency may be achieved with smaller droplets, higher electric fields, or forcing droplets to flow closer to the central separation wall. Improvements to bypass the presence of spikes at the oil–aqueous interface could include algorithmic detection within the microcontroller, the use of refractive-index matching oils, or the use of electronic low-pass filters. The direct detection of NADH formation is possible but challenging due to its low extinction coefficient (6,220 $M^{-1}{\cdot}cm^{-1}$ in water at 340 nm) as well as absorption losses within the fiber optics at this wavelength. However, the present setup allowed detection of 250 μM NADH (using a 365-nm LED light source).

Utility of Absorbance-Based Selections for Directed Evolution. The power of in vitro compartmentalization for the screening of enzyme activities has been demonstrated previously with several formats based on fluorescence-based readouts (7, 12–14, 18, 37–39) The development of the AADS module further extends the range of applications toward enzymes for which no fluorescent assays are available or where fluorescent reporters are only accessible by complicated organic synthesis. Even when a fluorogenic assay is available, absorbance detection may offer advantages: Typically fluorogenic moieties are large and hydrophobic and render substrates and products often insoluble, so that solubility effects obscure the readout of enzymatic turnover. The size of the typically large fluorogenic moiety may also divert directed evolution away from the structure of the desired substrate. In the specific case of amino acid dehydrogenases, the substrate CTC–formazan cannot be used in assays in solution, because it is only fluorescent in the solid state (40, 41).

The sorting of improved PheDH variants was demonstrated by driving the absorbance detection sorter at high, practically useful rates (~100 Hz). This throughput enables the analysis of 10^6 droplets within 3 h with a total reaction volume smaller than 200 μL, which offers a rapid and more economical strategy than any other conventional format [e.g., a more than half a million-fold smaller assay volume than microwell plate screening (14)]. Formation of absorbing product in the micromolar range can be readily detected given a high extinction coefficient (>30,000 $M^{-1}{\cdot}cm^{-1}$) and a water-soluble dye. Although we conducted selections under conditions typical for biocatalytic applications (i.e., at saturating substrate concentration $>K_M$, where a maximal turnover rate is achieved), experiments around K_M are also possible (as suggested by the clear separation of positives and negatives at [S] = 1 mM; see *SI Appendix*, Fig. S7).

The sorter we describe can detect ~10^9 molecules of the dye WST-1 formazan, which may be compared with close to a million enzyme copies produced in one *E. coli* cell (*SI Appendix*, *Text B*, Table S1, and Fig. S14) or >10^4 in in vitro expression (42). Based on this ratio, ~1,300 turnovers per enzyme molecule in the single-cell lysate assays used in this work are necessary to reach the detection limit, which does not impose unreasonable demands on enzyme proficiency. In the case of PheDH, the high activity of the enzyme leads to a robust phenotype, producing ~2 mM of product after 3 h. This means that enzymes with activities up to three orders of magnitude lower (k_{cat}/K_M ~100 $M^{-1}{\cdot}s^{-1}$) should still produce enough product to be amenable to selection by AADS within a reasonable time frame. Even conventional approaches that provide reasonable throughput (~10^5 per day), such as colony screening, are an order of magnitude slower than AADS and additionally compromised by low assay quality.

Protein engineering efforts, including directed evolution, are often hampered by inefficient expression and lack of stability of the target proteins (43, 44), so identifying variants with both enhanced soluble expression levels (i.e., increased kinetic protein stability) and long-term endurance in ultrahigh throughput suggests that this system is a useful enabling module of the microfluidic toolkit for enzyme improvement. An improvement of these properties via this workflow sets the scene for step-by-step (45) accumulation of mutations that enhance evolvability (46, 47) and allow adaptation of substrate specificity or introduction of mechanistic switches (48–51). The more robust quadruple mutant $PheDH^{V26I/N122S/L193M/T339I}$ will be useful to buffer the effects of the growing mutational load that carries a stability cost in future evolution rounds. The ability to increase the activity of selected PheDH variants toward L-Phe substantially in two rounds of directed evolution validates AADS for an enzyme class with valuable applications in large-scale processes: NADH-dependent enzymes are widely used in industry for the production of chiral amines (52). The ultrahigh throughput that is achievable with droplet microfluidics can now be applied to a wider circle of reactions, specifically NADPH cofactor-dependent enzymes. The ease by which the proverbially vast sequence space can be explored for these types of reactions that so far could only be evolved with lower throughput will increase the chances of success in their directed evolution.

Materials and Methods

Flow-Focusing Droplet Generation. A conventional droplet generator (height, 80 μm; width, 50 μm at the flow-focusing junction) was used to generate droplets at high rates (>1 kHz). Fluorinated oil HFE-7500 was purchased from 3M Novec and the surfactant (Picosurf1) from Dolomite Microfluidics. Chips were operated with syringe pumps (Nemesys, Cetoni) and gas-tight glass syringes (SGE). The flow rates for oil, cell preparation, and the lysis/substrate mix were 30 μL/min, 8 μL/min, and 8 μL/min, respectively.

Chip Fabrication. The sorting chip was designed with CAD software (DraftSight, Dassault Systems) and the device fabricated following classical soft-lithography procedures by using a high-resolution acetate mask (Microlithography Services Ltd.) and SU-8–2025 photoresist patterning (53). The resulting microchannels obtained in polydimethylsiloxane (PDMS) were plasma bonded on a thin cured PDMS layer (5 g PDMS in a Petri dish; Ø, 9 cm), flushed with 2% (vol/vol) Trichloro(1H,1H,2H,2H-perfluorooctyl)silane in HFE-7500, put in a 65 °C oven for 30 min, and the PDMS–PDMS devices then bonded to a microscope glass slide. Electrodes were made by filling channels with salt solution (5 M NaCl) as a practical alternative to low-melting point metals (54). Optical fibers (SMA Fiber Patch Cable, 50 microns, 0.22 NA; Thorlabs) were stripped (so that only the cladding was left) and manually inserted into the chip under a microscope. Alignment was tested by connecting one fiber to the fiber-coupled LED light source (M455F1, royal blue, Thorlabs) and the other to the photodetector (PDA36A, Thorlabs). Once proper alignment was obtained, the fibers were fixed with epoxy glue, and freshly degassed PDMS was inserted into the fiber channels through specific inlets to remove air, preventing the scattering of light (see *SI Appendix*, Fig. S1). The PDMS was left overnight at room temperature inside the channels for curing. Design files will be deposited on the DropBase (openwetware.org/wiki/DropBase).

Sorting Electronics. The voltage signal from the photodetector was split in two, recorded with a custom Labview program [using an Analog-to-Digital Converter (NI, USB-6009)], and at the same time sampled in 12-bit resolution via an analog-in pin of a 32-bit CortexM3 ARM-based microcontroller (Arduino Due). To match the voltage of the detector (max., 10 V) to the maximum voltage tolerable for the microcontroller board (3.3 V), a simple voltage divider (10 kΩ resistors) was used. On the microcontroller, the signal from the detector was compared with a threshold value for sorting. Below the threshold, a pin was set high to activate a pulse generator (TGP110, Thurlby Thandar Instruments), used to generate a 5-V pulse, and manually adjusted to be smaller than the droplet period (typically several milliseconds). The pulse generator controlled a function generator (20 MHz DDS Function Generator TG 2000, TTi) working in external gated mode, generating a 10-kHz square signal at an adjustable amplitude, which was then amplified 100 times with a voltage amplifier (TREK 601c) to actuate the sorter. This setup enabled convenient manual adjustment of all important sorting parameters.

Directed Evolution. The wtPheDH gene and its variants were cloned into pASK-IBA63b-plus (IBA) and expressed in fusion with a C-terminal Strep-tag. Gene libraries were generated by error-prone PCR (**Lib0**; 10^6 transformants; 1.7 mutations per gene) and StEP PCR (55) (**Lib1**; 10^6 transformants) for the first and the second round of directed evolution, respectively. The library variants were screened by compartmentalization of single *E. coli* cells, each expressing an individual library variant, in single droplets and sorted by AADS. Briefly, *E. coli* BL21(DE3) cells were transformed with the plasmids carrying the wtPheDH library variants. The cells were grown in suspension culture (LB, 100 μg/mL ampicillin) for protein expression under the control of the Tet promoter (200 ng/mL anhydrotetracyclin) and subsequently compartmentalized in single emulsions (ratio 1:2 for **Lib0** and 1:10 for **Lib1**) in 100 mM glycine–KOH buffer, pH 10, with substrates (10 mM L-Phe, 10 mM NAD^+, 5 mM WST-1, and 5 μg/mL mPMS, and 1 mM of WST-1 formazan as offset) and cell lysis agents [120 KU/mL rLysozyme and 4% (vol/vol) CelLytic B]. After collection in a syringe and incubation at room temperature (90 min), the droplets were injected into the AADS chip and sorted based on their absorbance at 455 nm using a defined selection threshold (see *SI Appendix*, Fig. S8). Plasmid DNA from collected droplets was recovered by de-emulsification using 1H,1H,2H,2H-perfluorooctanol, purified, and transformed into *E. coli* E. cloni 10G cells (Lucigen) by electroporation (18). After overnight growth on solid media (LB agar, 100 μg/mL ampicillin), plasmid DNA was extracted from the colonies and retransformed into *E. coli* BL21(DE3) cells for further colony- or 96-well-plate–based screenings. Details of screening procedures, expression analysis, purification, and characterization of selected hits are available in *SI Appendix*.

ACKNOWLEDGMENTS. This research was funded by the Engineering and Physical Sciences Research Council (studentship to R.H. and an Impact Acceleration Account Partnership Development Award), the Biological and Biotechnological Research Council (BBSRC), and Johnson Matthey. S.E. and M.F. were supported by postdoctoral Marie-Curie fellowships. F.H. is an ERC Investigator.

1. Bornscheuer UT, et al. (2012) Engineering the third wave of biocatalysis. *Nature* 485(7397):185–194.
2. Turner NJ (2009) Directed evolution drives the next generation of biocatalysts. *Nat Chem Biol* 5(8):567–573.
3. Bershtein S, Tawfik DS (2008) Advances in laboratory evolution of enzymes. *Curr Opin Chem Biol* 12(2):151–158.
4. Park HS, et al. (2006) Design and evolution of new catalytic activity with an existing protein scaffold. *Science* 311(5760):535–538.
5. Romero PA, Arnold FH (2009) Exploring protein fitness landscapes by directed evolution. *Nat Rev Mol Cell Biol* 10(12):866–876.
6. Lin H, Cornish VW (2002) Screening and selection methods for large-scale analysis of protein function. *Angew Chem Int Ed Engl* 41(23):4402–4425.
7. Colin PY, Zinchenko A, Hollfelder F (2015) Enzyme engineering in biomimetic compartments. *Curr Opin Struct Biol* 33:42–51.
8. Schaerli Y, Hollfelder F (2009) The potential of microfluidic water-in-oil droplets in experimental biology. *Mol Biosyst* 5(12):1392–1404.
9. Theberge AB, et al. (2010) Microdroplets in microfluidics: An evolving platform for discoveries in chemistry and biology. *Angew Chem Int Ed Engl* 49(34):5846–5868.
10. Baret JC, et al. (2009) Fluorescence-activated droplet sorting (FADS): Efficient microfluidic cell sorting based on enzymatic activity. *Lab Chip* 9(13):1850–1858.
11. Link DR, et al. (2006) Electric control of droplets in microfluidic devices. *Angew Chem Int Ed Engl* 45(16):2556–2560.
12. Zinchenko A, et al. (2014) One in a million: Flow cytometric sorting of single cell-lysate assays in monodisperse picolitre double emulsion droplets for directed evolution. *Anal Chem* 86(5):2526–2533.
13. Fischlechner M, et al. (2014) Evolution of enzyme catalysts caged in biomimetic gel-shell beads. *Nat Chem* 6(9):791–796.
14. Agresti JJ, et al. (2010) Ultrahigh-throughput screening in drop-based microfluidics for directed evolution. *Proc Natl Acad Sci USA* 107(9):4004–4009.
15. Colin P-Y, et al. (2015) Ultrahigh-throughput discovery of promiscuous enzymes by picodroplet functional metagenomics. *Nat Commun* 6:10008.
16. Sjostrom SL, et al. (2014) High-throughput screening for industrial enzyme production hosts by droplet microfluidics. *Lab Chip* 14(4):806–813.
17. Najah M, et al. (2014) Droplet-based microfluidics platform for ultra-high-throughput bioprospecting of cellulolytic microorganisms. *Chem Biol* 21(12):1722–1732.
18. Kintses B, et al. (2012) Picoliter cell lysate assays in microfluidic droplet compartments for directed enzyme evolution. *Chem Biol* 19(8):1001–1009.
19. Chen B, et al. (2016) High-throughput analysis and protein engineering using microcapillary arrays. *Nat Chem Biol* 12(2):76–81.
20. Bornscheuer UT (2016) Protein engineering: Beating the odds. *Nat Chem Biol* 12(2): 54–55.
21. Hall M, Bommarius AS (2011) Enantioenriched compounds via enzyme-catalyzed redox reactions. *Chem Rev* 111(7):4088–4110.
22. Kohls H, Steffen-Munsberg F, Höhne M (2014) Recent achievements in developing the biocatalytic toolbox for chiral amine synthesis. *Curr Opin Chem Biol* 19:180–192.
23. Ahn K, et al. (2006) Dielectrophoretic manipulation of drops for high-speed microfluidic sorting devices. *Appl Phys Lett* 88(2):024104.
24. Courtois F, et al. (2009) Controlling the retention of small molecules in emulsion microdroplets for use in cell-based assays. *Anal Chem* 81(8):3008–3016.
25. Tokuriki N, Stricher F, Schymkowitz J, Serrano L, Tawfik DS (2007) The stability effects of protein mutations appear to be universally distributed. *J Mol Biol* 369(5): 1318–1332.
26. Chennamsetty N, Voynov V, Kayser V, Helk B, Trout BL (2009) Design of therapeutic proteins with enhanced stability. *Proc Natl Acad Sci USA* 106(29):11937–11942.
27. Kramer RM, Shende VR, Motl N, Pace CN, Scholtz JM (2012) Toward a molecular understanding of protein solubility: Increased negative surface charge correlates with increased solubility. *Biophys J* 102(8):1907–1915.
28. Kataoka K, et al. (1993) Site-directed mutagenesis of a hexapeptide segment involved in substrate recognition of phenylalanine dehydrogenase from Thermoactinomyces intermedius. *J Biochem* 114(1):69–75.
29. Sciambi A, Abate AR (2015) Accurate microfluidic sorting of droplets at 30 kHz. *Lab Chip* 15(1):47–51.
30. Srinivasan V, Pamula VK, Fair RB (2004) An integrated digital microfluidic lab-on-a-chip for clinical diagnostics on human physiological fluids. *Lab Chip* 4(4):310–315.
31. Trivedi V, et al. (2010) A modular approach for the generation, storage, mixing, and detection of droplet libraries for high throughput screening. *Lab Chip* 10(18): 2433–2442.
32. Deal KS, Easley CJ (2012) Self-regulated, droplet-based sample chopper for microfluidic absorbance detection. *Anal Chem* 84(3):1510–1516.
33. Gielen F, et al. (2013) A fully unsupervised compartment-on-demand platform for precise nanoliter assays of time-dependent steady-state enzyme kinetics and inhibition. *Anal Chem* 85(9):4761–4769.
34. Choi K, Mudrik JM, Wheeler AR (2015) A guiding light: Spectroscopy on digital microfluidic devices using in-plane optical fibre waveguides. *Anal Bioanal Chem* 407(24): 7467–7475.
35. Rushworth CM, Jones G, Fischlechner M, Walton E, Morgan H (2015) On-chip cavity-enhanced absorption spectroscopy using a white light-emitting diode and polymer mirrors. *Lab Chip* 15(3):711–717.
36. Novak L, Neuzil P, Pipper J, Zhang Y, Lee S (2007) An integrated fluorescence detection system for lab-on-a-chip applications. *Lab Chip* 7(1):27–29.
37. Griffiths AD, Tawfik DS (2003) Directed evolution of an extremely fast phosphotriesterase by in vitro compartmentalization. *EMBO J* 22(1):24–35.
38. Aharoni A, Amitai G, Bernath K, Magdassi S, Tawfik DS (2005) High-throughput screening of enzyme libraries: Thiolactonases evolved by fluorescence-activated sorting of single cells in emulsion compartments. *Chem Biol* 12(12):1281–1289.
39. Mastrobattista E, et al. (2005) High-throughput screening of enzyme libraries: In vitro evolution of a beta-galactosidase by fluorescence-activated sorting of double emulsions. *Chem Biol* 12(12):1291–1300.
40. Huang Z, et al. (2000) Rapid detection of Zymomonas mobilis redox activity using 5-cyano-2,3-tolyl-tetrazolium chloride (CTC). *Biotechniques* 29(3):424–425, 428.
41. Gruden CL, Fevig S, Abu-Dalo M, Hernandez M (2003) 5-Cyano-2,3-ditolyl tetrazolium chloride (CTC) reduction in a mesophilic anaerobic digester: Measuring redox behavior, differentiating abiotic reduction, and comparing FISH response as an activity indicator. *J Microbiol Methods* 52(1):59–68.
42. Courtois F, et al. (2008) An integrated device for monitoring time-dependent in vitro expression from single genes in picolitre droplets. *ChemBioChem* 9(3):439–446.
43. Bloom JD, Arnold FH (2009) In the light of directed evolution: Pathways of adaptive protein evolution. *Proc Natl Acad Sci USA* 106(Suppl 1):9995–10000.
44. Socha RD, Tokuriki N (2013) Modulating protein stability—Directed evolution strategies for improved protein function. *FEBS J* 280(22):5582–5595.
45. Tracewell CA, Arnold FH (2009) Directed enzyme evolution: Climbing fitness peaks one amino acid at a time. *Curr Opin Chem Biol* 13(1):3–9.
46. Bloom JD, Labthavikul ST, Otey CR, Arnold FH (2006) Protein stability promotes evolvability. *Proc Natl Acad Sci USA* 103(15):5869–5874.
47. Tokuriki N, Stricher F, Serrano L, Tawfik DS (2008) How protein stability and new functions trade off. *PLOS Comput Biol* 4(2):e1000002.
48. O'Brien PJ, Herschlag D (1999) Catalytic promiscuity and the evolution of new enzymatic activities. *Chem Biol* 6(4):R91–R105.
49. Renata H, Wang ZJ, Arnold FH (2015) Expanding the enzyme universe: Accessing non-natural reactions by mechanism-guided directed evolution. *Angew Chem Int Ed Engl* 54(11):3351–3367.
50. Bornscheuer UT, Kazlauskas RJ (2004) Catalytic promiscuity in biocatalysis: Using old enzymes to form new bonds and follow new pathways. *Angew Chem Int Ed Engl* 43(45):6032–6040.
51. Toscano MD, Woycechowsky KJ, Hilvert D (2007) Minimalist active-site redesign: Teaching old enzymes new tricks. *Angew Chem Int Ed Engl* 46(18):3212–3236.
52. Kroutil W, et al. (2013) Asymmetric preparation of prim-, sec-, and tert-amines employing selected biocatalysts. *Org Process Res Dev* 17(5):751–759.
53. Xia YN, Whitesides GM (1998) Soft lithography. *Angew Chem* 37(5):550–575.
54. Sciambi A, Abate AR (2014) Generating electric fields in PDMS microfluidic devices with salt water electrodes. *Lab Chip* 14(15):2605–2609.
55. Zhao H, Giver L, Shao Z, Affholter JA, Arnold FH (1998) Molecular evolution by staggered extension process (StEP) in vitro recombination. *Nat Biotechnol* 16(3): 258–261.

Supporting Information

Gielen et al. 10.1073/pnas.1606927113

Movie S1. Live demonstration of the absorbance chip. Mixtures of droplets containing PBS buffer only and droplets with a strongly absorbing black food dye diluted in the same buffer were generated, stored in a tubing and reinjected into the sorting device. The video shows the sorting of droplets containg black dye. Flow rates were 40 μL/min for the respacing oil phase and 4 μL/min for the emulsion droplets, sorting voltage was 600 V peak-to-peak at 10 kHz for 5 ms and the frequency of droplets was around 80 Hz.

Movie S1

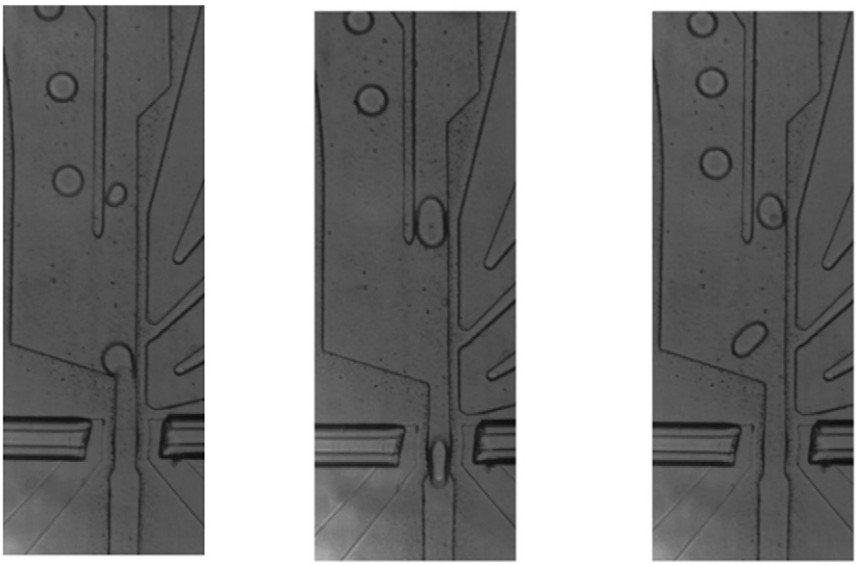

Movie S2. Video examples of droplets sorted as false positives. (left) A small satellite droplet. (middle) Two consecutive droplets creating a double edge scatter. (right) Droplet containing a dust particle. All droplets contained 10 mM L-Phe, 10 mM NAD^+, 5 mM WST-1 and 5 μg/mL mPMS and 1 mM of WST-1 formazan as an offset, in 100 mM glycine-KOH buffer, pH 10, voltage was 600 V peak-to-peak, 10 kHz, 5 ms. Flow rates: 40 μL/min for the oil phase and 2 μL/min for the emulsion droplets.

Movie S2

Movie S3. Short example video clips of 10 different droplets sorted during a library sorting experiment. All droplets contained 10 mM L-phe, 10 mM NAD^+, 5 mM WST-1 and 5 μg/mL mPMS and 1 mM of WST-1 formazan as an offset, in 100 mM glycine-KOH buffer, pH 10, voltage was 600 V peak-to-peak, 10 kHz, 5ms. Flow rates: 40 μL/min for the oil phase and 2 μL/min for the emulsion droplets.

Movie S3

Other Supporting Information Files

SI Appendix (PDF)

Supporting Information for

Ultrahigh-Throughput Directed Enzyme Evolution by Absorbance-Activated Droplet Sorting (AADS)

Fabrice Gielen,[†§] Raphaelle Hours,[†§] Stephane Emond,[†] Martin Fischlechner,[†‡] Ursula Schell,[#] Florian Hollfelder[†*]

[†] Department of Biochemistry, University of Cambridge, 80 Tennis Court Road, Cambridge, CB2 1GA, United Kingdom
[‡] Institute for Life Sciences, University of Southampton, Southampton SO17 1BJ, United Kingdom
[#] Johnsson Matthey Catalysis and Chiral Technologies, 28, Cambridge Science Park, Milton Road, Cambridge CB4 0FP, United Kingdom

[*] Corresponding author: E-mail: fh111@cam.ac.uk. Phone: +44-1223766048

[§] These authors contributed equally to this work.

1. SI Text

1.1 Detailed Materials and Methods

Bacterial strains, plasmids, enzymes and chemicals

Proteins were expressed in the *E. coli* strain BL21(DE3). Electrocompetent *E. coli* strain E.cloni 10G (Lucigen) was used for the construction of directed evolution libraries and DNA recovery from single emulsions. Plasmid pASK-IBA63b-plus (High copy plasmid, IBA, Germany) was used for the expression of *Rhodococcus* sp. M4 PheDH (wtPheDH; Uniprot ID Q59771) in fusion with a C-terminal Strep-tag. Unless indicated otherwise, all DNA modifying enzymes were from Thermo Fisher Scientific and used according to the manufacturer's instructions. Chemicals used in this study were all purchased from Sigma-Aldrich unless indicated otherwise.

Construction of directed evolution libraries

In the first round of directed evolution, the wtPheDH gene was randomly mutated by error-prone PCR, using Mutazyme II low-fidelity polymerase (Stratagene) with an average of 1.7 mutations per gene. The resulting PCR product was ligated into pASK-IBA63b-plus at NcoI and XhoI sites. The ligation products were then transformed into electrocompetent *E. coli* E.cloni 10G cells, yielding library **Lib0** (~10^6 transformants). For the second round of evolution, a shuffling library (dubbed **Lib1**) was prepared using StEP PCR (1) by recombining six hits (V26I, Q45H, T13N/L193M, T121I and N122S/T339I) from the first round of screening. The reaction was performed using 0.15 pmol of the total template plasmid pool with BioTaq DNA polymerase (Bioline), 0.6 µM of each primer, 0.2 mM of each dNTPs and 1.5 mM of $MgCl_2$. The PCR program was performed as previously described (1). Subsequent cloning steps were carried out as described above to yield library **Lib1** (~10^6 transformants).

Preparation of cells for compartmentalization and lysis in droplets

For the expression of wtPheDH and its variants, *E. coli* BL21(DE3) cells were initially grown overnight at 37°C in 5 mL LB broth supplemented with ampicillin (Amp; 100 µg/mL). 5 mL LB-Amp medium containing ampicillin (100 µg/mL) were inoculated with this starter culture at a ratio 1:20. After 2 h of growth at 37°C,

protein expression was induced by addition of anhydrotetracyclin (AnhTet; 200 ng/mL) and growth at 20 °C for 16 h. After expression, OD600 was measured to determine the cell density (an OD600 of 1 is equivalent to ~5 x 10^8 cells/mL) and the culture was diluted to enable encapsulation at occupancies of 1 cell per droplet. This diluted cell suspension was then mixed with the density-matching agent Percoll (final concentration: 25%, v/v) in 100 mM glycine-KOH buffer, pH 10 and taken up into a syringe. A second syringe contained a mixture of substrate (10 mM L-Phe, 10 mM NAD^+, 5 mM WST-1 and 5 µg/mL mPMS and 1 mM of WST-1 formazan as an offset, in 100 mM glycine-KOH buffer, pH 10) and cell lysis agents (rLysozyme 4 µL/mL Novagen (30 KU/µl), and CelLytic™ B (4% (v/v) of 10× stock) in 100 mM glycine-KOH buffer pH10). This procedure was used for the screening of directed evolution libraries. For model enrichment experiments, two cultures were grown separately: one for the expression of wtPheDH and the other for the expression of P91 (not active on L-Phe) (2). After determining the cell density, these cultures were mixed to a ratio of 1:5000 (wtPheDH : P91) and diluted prior to droplet encapsulation as described.

DNA recovery from droplets by transformation

Sorted droplets (representing a typical total volume of ~180 pL) were de-emulsified by addition of 200 µL 1H,1H,2H,2H-perfluorooctanol (PFO), to achieve phase separation. After the removal of the top layer (i.e. the aqueous layer containing DNA) the bottom layer (containing PFO in oil) was again extracted with 200 µL double-distilled water to recover any remaining DNA. The harvested plasmid DNA was recovered from the combined aqueous layers using a spin column (DNA Clean & Concentrator-5, Zymo Research), eluting in 7 µL of elution solution from the kit. The purified DNA was then transformed into *E.coli* E. cloni 10G cells by applying one electric pulse of 1.80 kV (using an *E. coli* Pulser Cuvette, 0.1 cm electrode; Bio-Rad and MicroPulser). Sterile S.O.C Medium (275 µL, Invitrogen) was added and the transformed cells were incubated for 40 min at 37 °C, before being plated on LB-Amp agar and grown overnight at 37 °C. The transformation efficiency was determined by comparison of the number of colonies obtained after transformation to the number of sorted droplets. The plasmid DNA corresponding to the collected

wtPheDH variants was then extracted from the colonies and used to transform *E. coli* BL21(DE3) cells for further screens on colonies or in microplate format.

Screening procedures in microplates and on colonies

For screening in microplate format, *E. coli* BL21(DE3) transformants were individually picked and grown overnight in 300 µL LB-Amp at 37 °C in 96 deep-well plates. 25 µL of these cultures were used to inoculate 500 µL LB-Amp in 96 deep-well plates. After 2 hours of growth at 37 °C, protein expression was induced by adding AnhTet (to a final concentration of 200 ng/mL) and cells were further grown overnight at 20 °C. Cells were then pelleted by centrifugation at 4°C at maximum speed (3320×g) for 5-10 minutes and the supernatant removed. Pellets were frozen at -80 °C for 30 min and, after thawing, lysed by addition of 200 µL of lysis buffer (25 mM Tris-HCl pH 7.5, 0.1% Triton X100, 100 µg/mL rLysozyme (Novagen) and 0.8 U/mL benzonase (Novagen)). After 30 minutes of lysis, cell debris was spun down at 4 °C at 3320×g for 20 minutes. Enzyme assays were performed in 96-well plates containing a volume of 200 µL per well (20 µL pre-diluted lysate + 180 µL of 10 mM L-Phe, 10 mM NAD^+, 5 mM INT and 5 µg/mL mPMS in 100 mM glycine-KOH buffer pH10). The reactions were monitored by recording the absorbance at 495 nm.

For colony screens, transformed *E. coli* BL21(DE3) cells (on average 500-2,000 CFU) were plated on LB-amp agar. The colonies were replicated with a sheet of filter paper (BioTrace NT Pure Nitrocellulose Transfer Membrane 0.2 µm, PALL Life Sciences) that was applied to the plate to print a replica and then placed onto a second plate containing LB-amp agar with 200 ng/mL AnhTet. After expression overnight at 20°C, the filter paper was placed into an empty Petri dish and cells were lysed prior to the activity assay by alternating three times between storage at -20°C and 37°C. Subsequently, a layer of top agar (0.5% agar in 100 mM glycine-KOH pH 10) containing the substrates (10 mM L-Phe, 10 mM NAD^+, 5 mM INT and 5 µg/mL mPMS) was applied and the emrgence of red color (resulting from the formation of INT-Formazan) monitored after 30 minutes.

These procedures were the basis of the determination of enrichment ratios and also used to identify hits after droplet sorting during directed evolution experiments.

Protein expression analysis

The mutants were transformed and expressed in *E.coli* BL21(DE3) overnight at 20 °C in 5 mL liquid cultures (containing anhydrotetracyclin, 200 ng/mL). 500 µL of the resulting cell suspension were pelleted. The pellets were resuspended in 50 µL of lysis solution (BugBuster protein extraction reagent from Merck Millipore (10:1 diluted in water) and lysonase bioprocessing reagent from Merck Millipore (3 µL/m)), and incubated at room temperature for one hour. Cell debris was pelleted and the soluble fractions were collected. 2 µL of each soluble fraction were analysed by SDS-PAGE (12%, run at 200 V for 1 hour; see Fig. S11). The pellets containing the insoluble fractions were washed with a 5-fold diluted lysis solution (see above) ; and 2 µL of each were analysed side-by-side by SDS-PAGE. The amount of expressed protein was quantified by densitometric analysis (ImageJ) of the corresponding band on the gel in Fig. S11.

Protein purification procedures

After expression in 200 mL liquid cultures, *E. coli* BL21(DE3) cells expressing wtPheDH or its variants were harvested by centrifugation and resuspended in 10 mL of lysis buffer (100 mM Tris-HCl pH 8.0, 150 mM NaCl, 1× Bugbuster™ protein extraction reagent (Merck Millipore), 3 µL/mL lysonase™ bioprocessing reagent (Merck Millipore) and EDTA-free protease inhibitors). Cell debris was removed by centrifugation (30,000×g, 1 h, 4 °C) and the clarified lysate was directly loaded onto Strep-Tactin Superflow resin (IBA Life). Strep-tagged wtPheDH proteins were eluted with Elution buffer (100 mM, pH 8.0, containing 150 mM NaCl and 2.5 mM d-desthiobiotin) according to the manufacturer's instructions. Eluted proteins were concentrated to a final volume of 1 ml and buffer exchange was performed using PD MiniTrap G-25 Spin columns from GE Healthcare with 100 mM phosphate buffer pH 7. All the identified hits were purified using this procedure, with the exception of two 2nd round variants (V26I/N122S/T339I and Q45H/N122S/L193M), which aggregated during the purification process.

Kinetic characterization of PheDH variants

Enzymatic assays were performed at 25 °C in a final volume of 200 µL of 100 mM glycine-KOH pH 10 under saturating conditions of NAD+ (5 mM) and a range of L-Phe concentrations (0.2-60 mM). Purified protein was diluted to a concentration of 10

nM. Initial velocities (v_0) were determined by monitoring NADH formation at 340 nm. Kinetic parameters were obtained by fitting initial rates v_0 to the Michaelis-Menten with substrate inhibition using Kaleidagraph (Synergy Software): $v = k_{cat}[S] / (K_M + [S] + ([S]^2 / K_i))$ (3). Example data and details of equations used for fitting are shown in Fig. S12.

Differential scanning fluorimetry

2 μM of the purified enzymes (wtPheDH and variants V26I/L193M and V26I/N122S/L193M/T339I) were mixed with Sypro Orange protein gel stain (from Invitrogen), in two different buffers: 2× in MOPS (100 mM, NaCl 150 mM, pH 8) or Glycine-KOH (100 mM, pH 10). The samples were denatured by increasing the temperature from 25 to 80 °C using the Corbett Life Science Rotor-gene 6000, and the fluorescence of the Sypro orange was measured ($\lambda_{excitation}$ = 410 nm, $\lambda_{emission}$ = 610 nm). The T_m (defined as the temperature at which half of the enzyme population is denatured) corresponds to the first derivative for each temperature-fluorescence curve.

Kinetics of thermal inactivation

Half-lives of thermal inactivation were determined for purified wtPheDH and the two most thermostable variants (V26I/L193M and V26I/N122S/L193M/T339I) by incubating the enzymes (2 μM) at 50°C for various time intervals. Initial and residual activities were measured at 20°C in glycine-KOH buffer 100 mM, pH 10, by measuring the NADH production at 340 nm with a spectrophotometer. The first-order rate constant, k_d, of irreversible thermal denaturation was obtained from the slope of the linear plots of ln (initial v_0/residual v_0) *versus* time (measured at [L-Phe]=10 mM), and the half-lives ($t_{1/2}$) were calculated as ln2/ k_d.

Activity *versus* temperature profiles

Initial specific activities of the purified wtPheDH and the two most thermostable variants (V26I/L193M and V26I/N122S/L193M/T339I) were measured at temperatures ranging from 30 to 65 °C, in glycine-KOH buffer (100 mM, pH 10, with 10 mM L-Phe and 5 mM NAD^+), by following the NADH production at 340 nM with a spectrophotometer.

2. Supplementary Data

A. Operation of the droplet sorter

A.1 Theoretical sensitivity of the absorbance detection

The percentage of transmission that could be reliably detected was 0.3% based on the noise level (30 mV) when working close to the saturation voltage of the detector (10 V). Therefore, at fixed pathlength (here 50 μm), given the extinction coefficient of WST-1 formazan (ε^{455nm} =34660 M^{-1} cm^{-1} at pH 10 in glycine-KOH buffer, 100 mM, measured at 455 nm), and applying the Beer-Lambert law, the estimated detection limit would be ~7.5 μM.

A.2 Fluidics

Sorting large droplets require higher electric fields because they experience a higher drag force. Although the dielectrophoretic force scales with the volume of the droplets, the large distance between droplets and electric field maximum (>100 μm) means this bulk force is not significantly higher than for smaller droplets flowing closer to the electrodes. Additionally, increases in the flow rate of the spacing oil was found to push droplets further away from the central separation wall. This means that the emulsion-to-oil ratio could be increased at high oil flow rates without affecting the sorting operation and, for instance, was 1:10 at 40 μL/min. This is useful for reducing the flow rate of the oil and therefore increase throughput further while reducing the total volume of respacing oil needed.

A.3 Assessment of leakage

Droplets with buffer only and droplets containing WST-1 (5 mM), mPMS (5 μg/mL) and NADH (5 mM) were co-generated in a microfluidic device with two flow-focussing channels converging to a single outlet and incubated together in tubing. The carrier phase was HFE-7500 containing 1.5% Picosurf 1 (w/w). The absorbance of droplets was measured several times during incubation for 0-4 hours by passing them though the detection module at arbitrary intervals. No increase in the absorbance of buffer droplets was observed within detection sensitivity (~10 μM) confirming the absence of detectable leakage.

A.4 Triggering droplet selection based on absorbance signals

Droplets containing glycine buffer (pH 9.85) only and buffer with WST-1 formazan (100 μM) were co-generated (See A.3 above) and their absorbance measured in the microfluidic sorting chip (Fig. 1A). A threshold was applied based on the second scattering edge to distinguish droplets containing WST-1 from those that did not. Below 100 μM WST-1 the edges mask the real absorbance value and droplets cannot be distinguished, which defines this concentration as the threshold for triggering a sorting signal. To circumvent this limitation, WST-1 formazan (1 mM) was added to the samples, resulting in a signal which can be triggered more sensitively (see Fig. 2B and Fig. S4).

A.5 Code for the Arduino Due microcontroller

The following code was used to read the analog signal coming from the photodetector and compare it to an arbitrary value (sortValue). When the sensor value (sensorValue) was lower than the sort value, it triggered a digital output (D13) to the high state.

```
int triggerPin = 13;
float sortValue=7.5;  // arbitrary voltage threshold
void setup() {
  pinMode(triggerPin, OUTPUT);
  Serial.begin(115200);
analogReadResolution(12);
}
void loop() {
   // read the input on analog pin 0:
  int sensorValue = analogRead(A0);
  float voltage = sensorValue * (3.33 / 4096.0);
  if (voltage<(sortValue/3))
  {
```

```
  digitalWrite(triggerPin,HIGH);
  delay(2);
}
  else
  digitalWrite(triggerPin,LOW);
}
```

B. Calculation of the number of soluble enzyme molecules per cell

The initial rates v_0 were measured (Table S1, column[a]) for different dilutions of cell lysate (*E. coli* BL12 (DE3)) expressing wtPheDH. The quantity of pure enzyme corresponding to each initial rate was determined according to a titration curve (Fig. S14). The number of molecules for each enzyme concentration was then calculated and divided by the number of cells to assess the average number of enzyme molecules per cell (Table S1, columns[b,c,d,e]).

References

1. Zhao H, Giver L, Shao Z, Affholter JA, & Arnold FH (1998) Molecular evolution by staggered extension process (StEP) in vitro recombination. *Nat Biotechnol* 16(3):258-261.
2. Colin P-Y, *et al.* (2015) Ultrahigh-throughput discovery of promiscuous enzymes by picodroplet functional metagenomics. *Nature Communications* 6:10008.
3. Cornish-Bowden A (2004) *Fundamentals of Enzyme Kinetics* (Portland Press (London)) p 438.

3. Supplementary Figures and /Tables

A

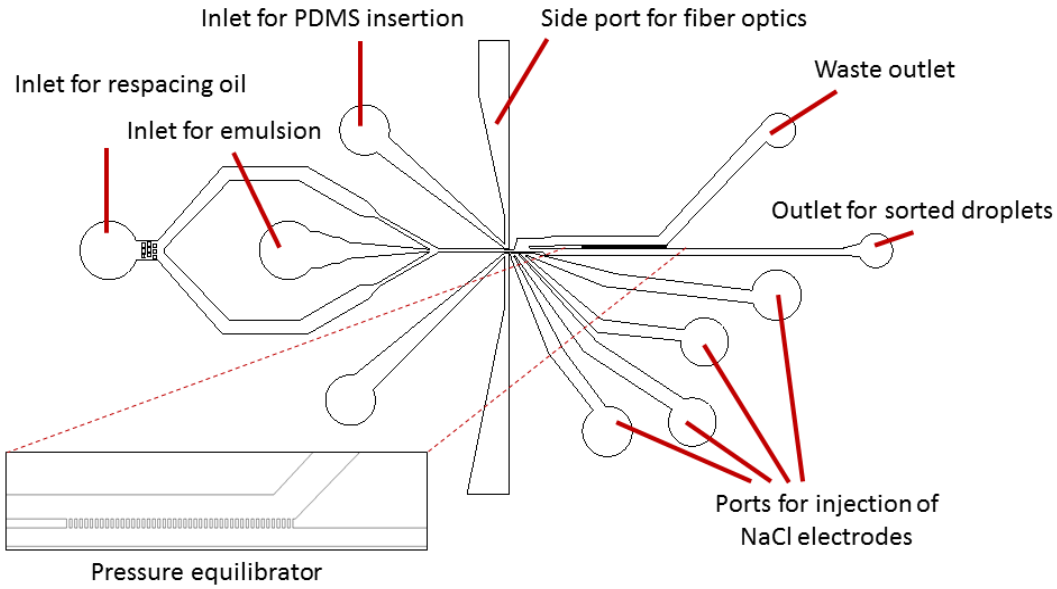

B

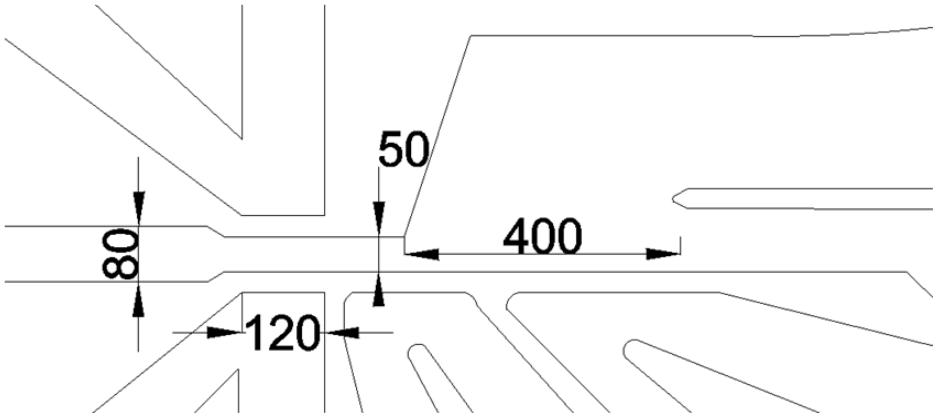

Fig. S1 Chip design. A. CAD drawing of the absorbance sorting chip displaying the side access ports for the fiber optics, inlets for spacing oil and emulsion as well as electrode channels and outlets for both waste and sorted droplets. **B.** Close-up view of the sorting junction with dimensions quoted in microns.

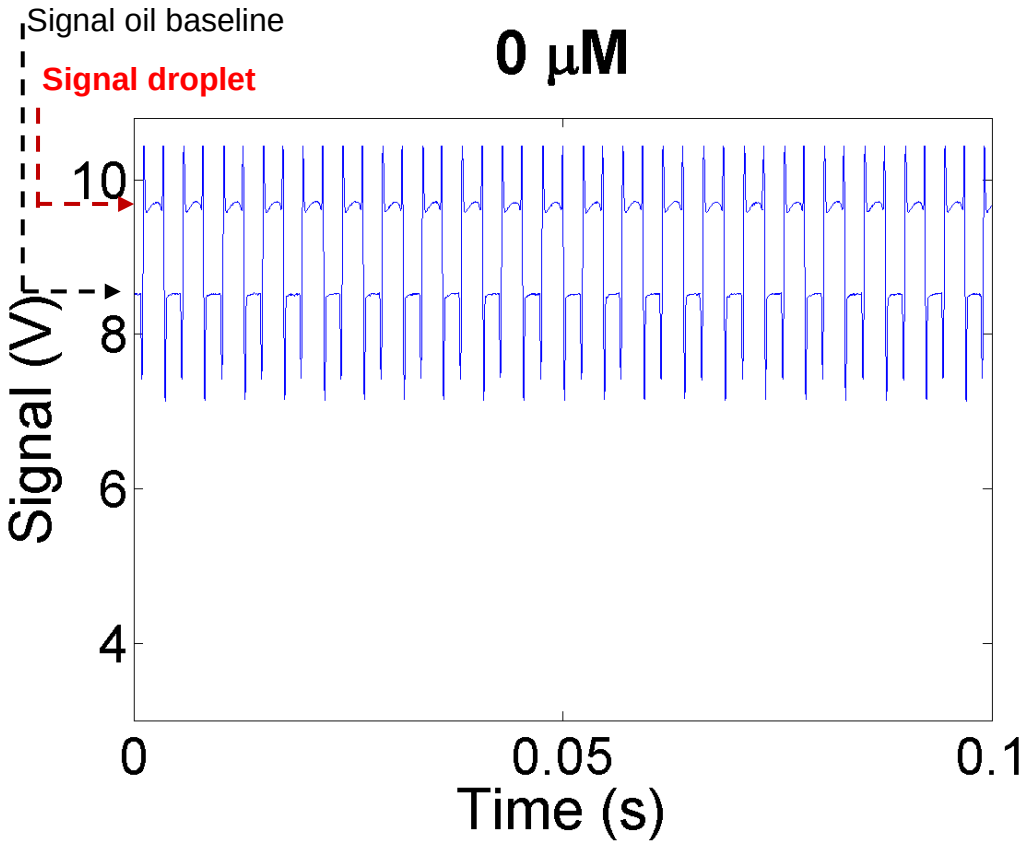
Signal oil baseline
Signal droplet
0 μM
Signal (V)
10
8
6
4
0
0.05
0.1
Time (s)

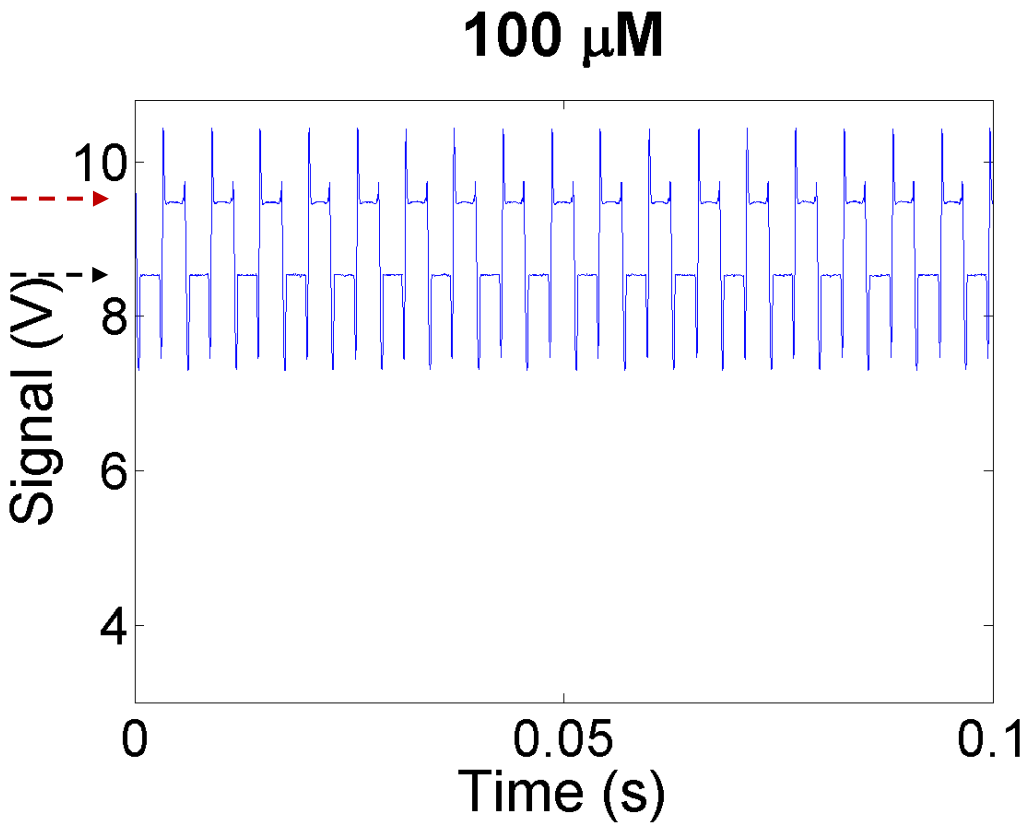
100 μM
10
8
6
4
Signal (V)
0
0.05
0.1
Time (s)

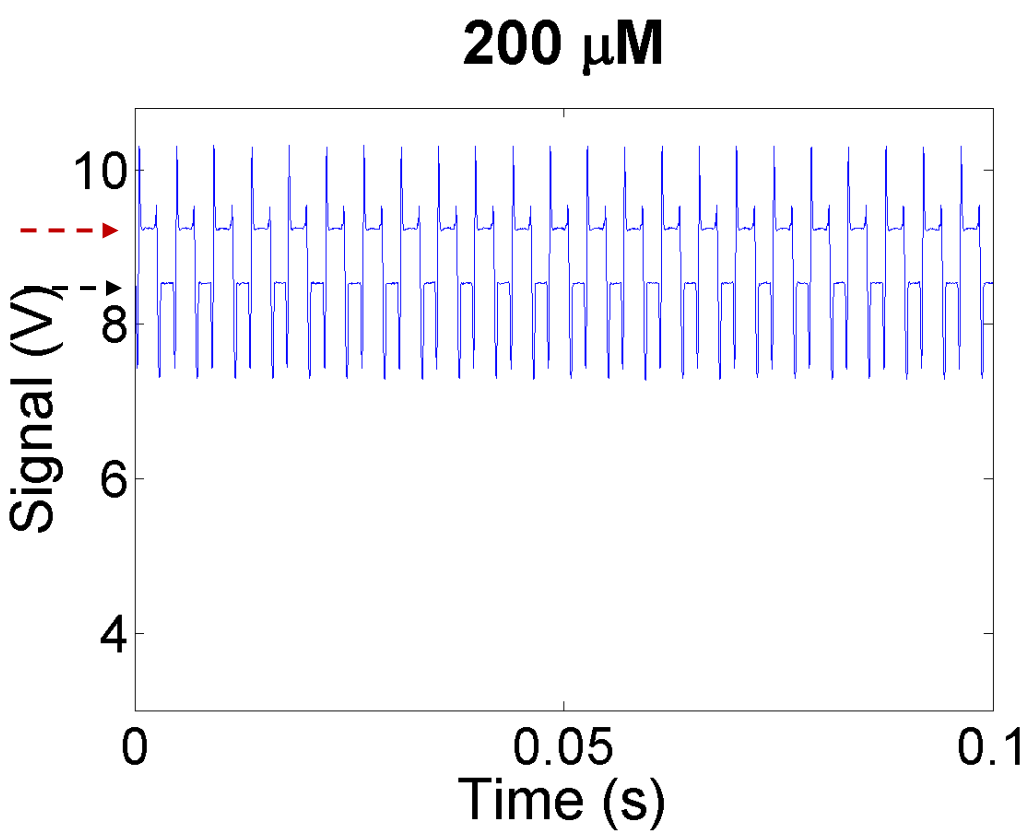
200 μM
10
8
6
4
Signal (V)
0
0.05
0.1
Time (s)

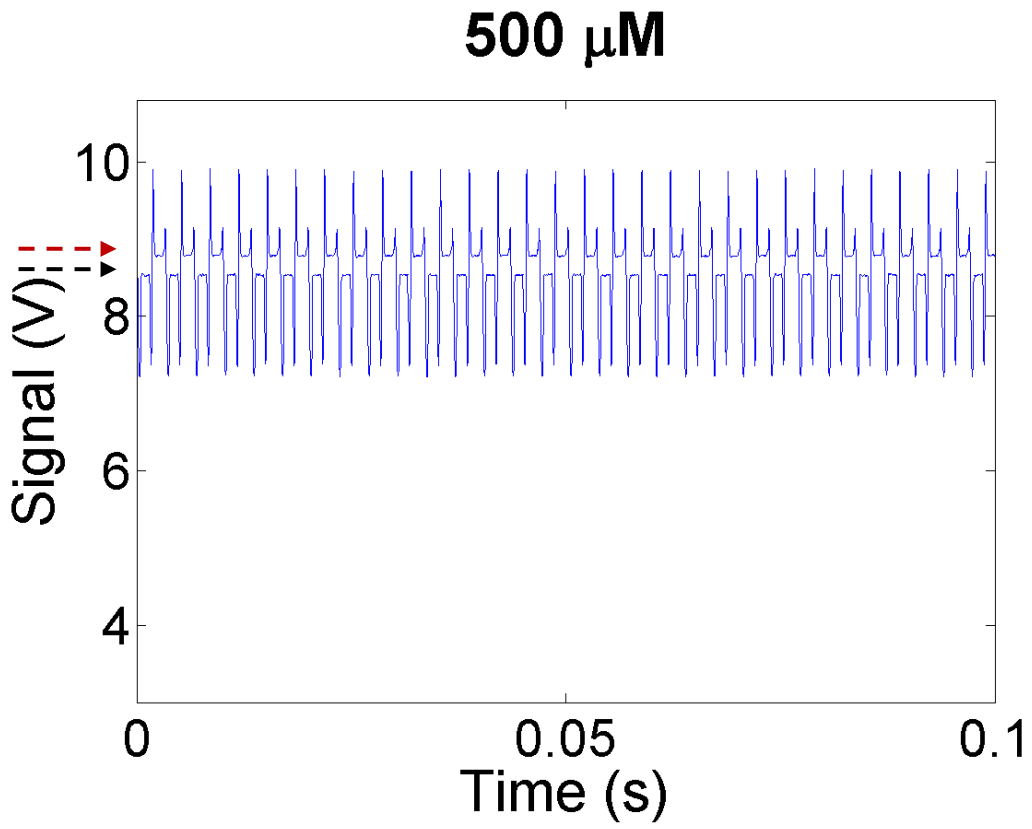
500 μM
10
8
6
4
Signal (V)
0
0.05
0.1
Time (s)

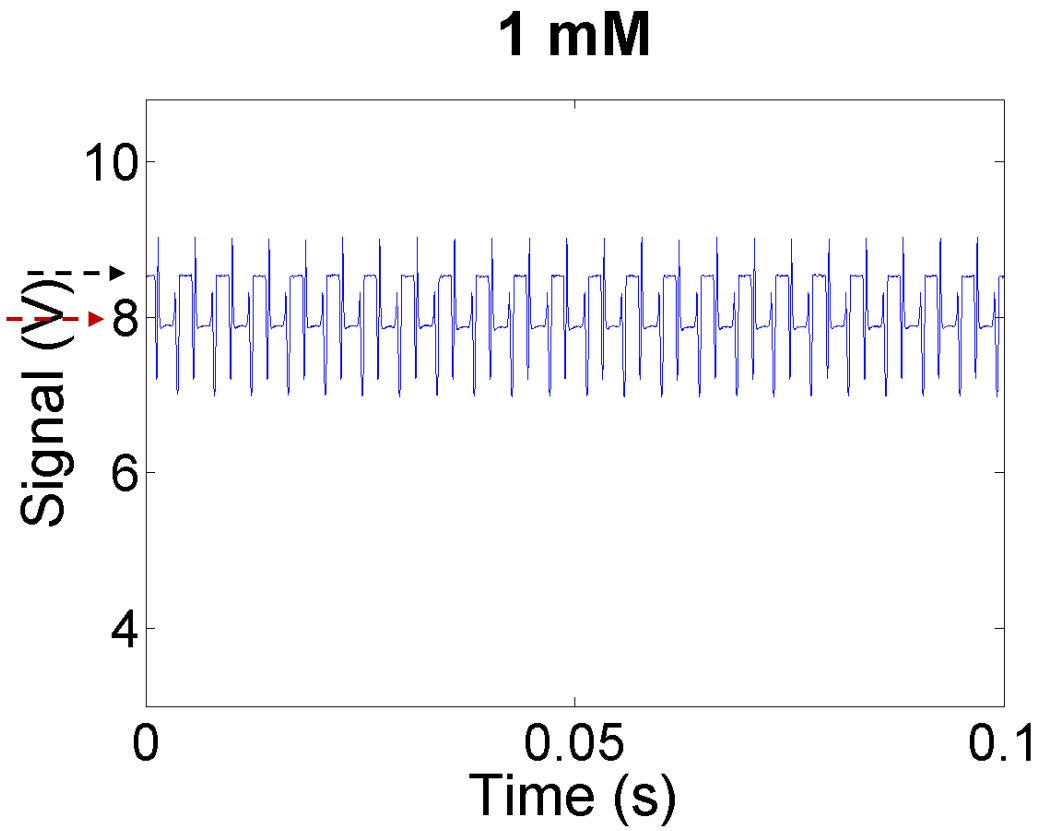
1 mM
10
8
6
4
Signal (V)
0
0.05
0.1
Time (s)

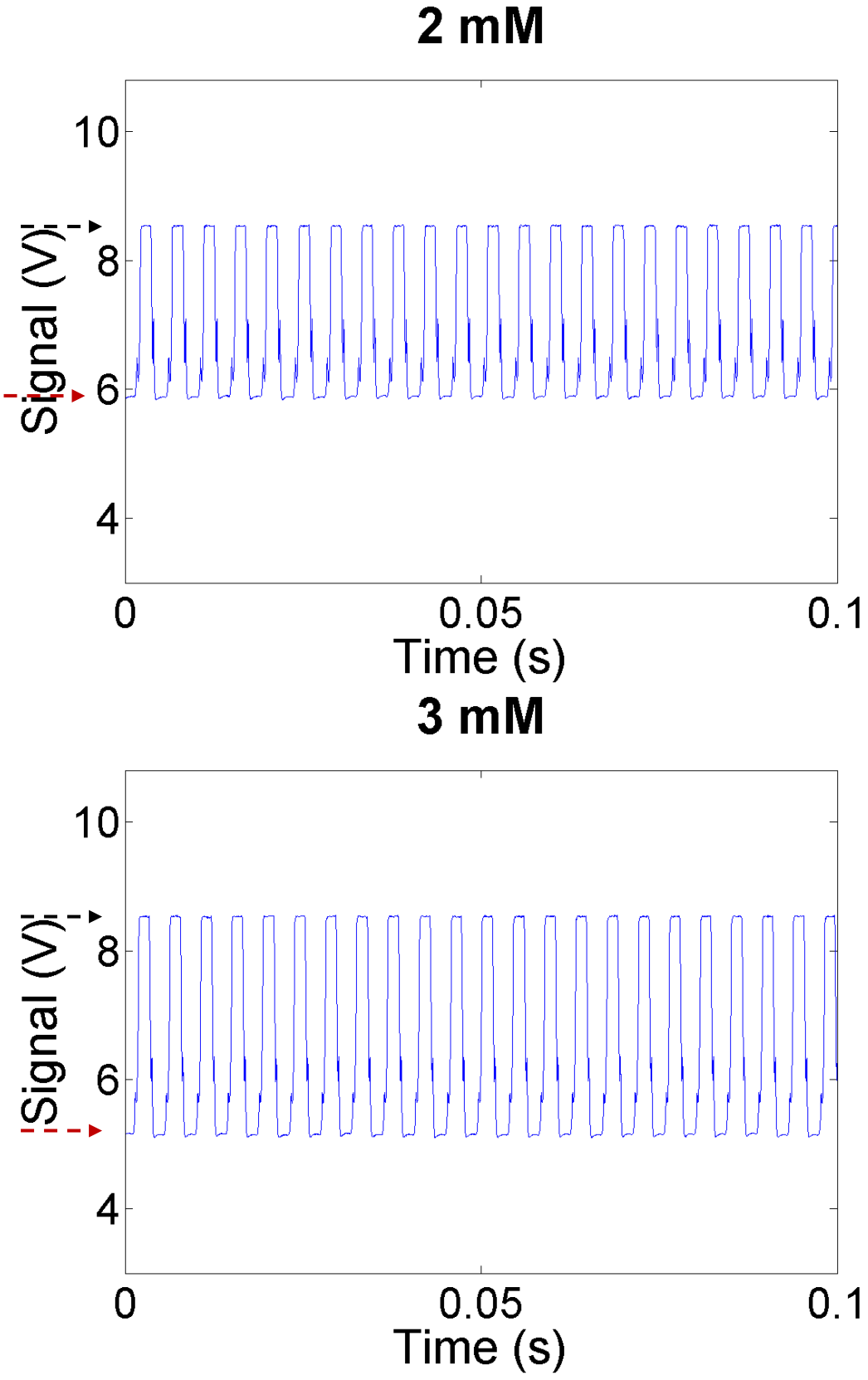
2 mM
10
8
6
4
Signal (V)
0
0.05
0.1
Time (s)
3 mM
10
8
6
4
Signal (V)
0
0.05
0.1
Time (s)

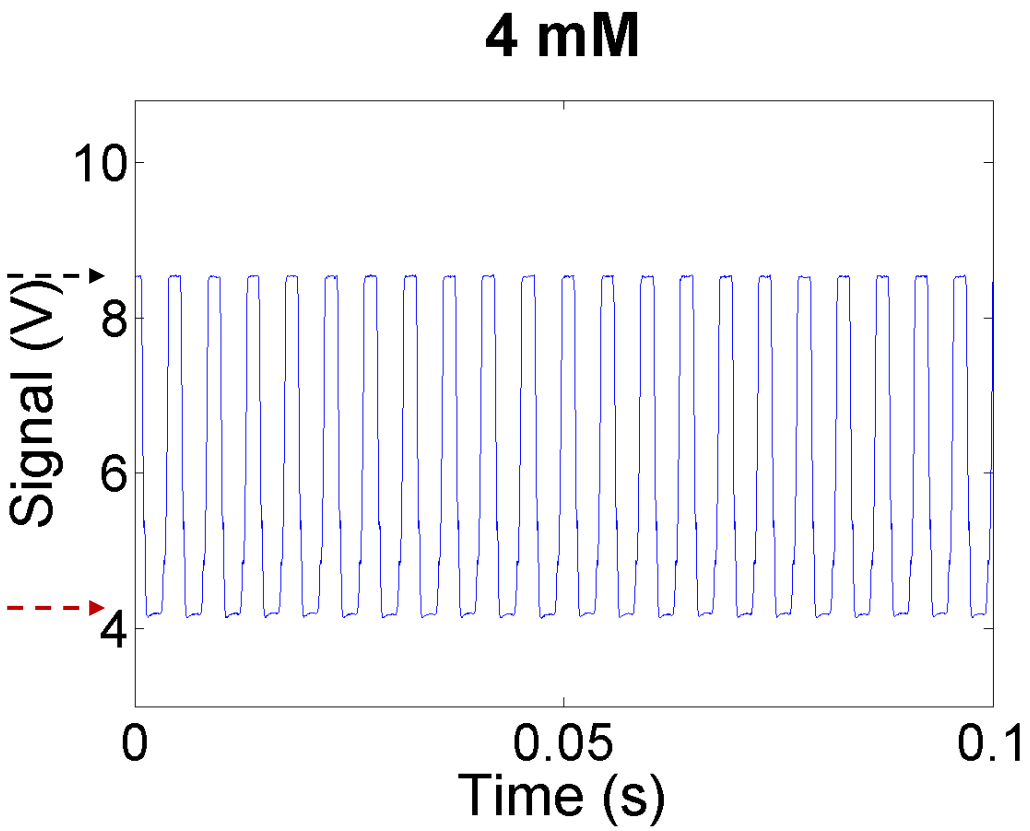

Fig S2. Time traces for calibration of the absorbance detector. Oil baseline and droplet signal are represented by dashed black and red arrows, respectively. Between 500 µM and 1 mM the positions of the black and red arrows are inverted, as the oil baseline is constant, but the droplet signal decreases (with increasing product concentration). The regularity of the time traces suggests stability of the readout and therefore suitability of quantitative assessments.

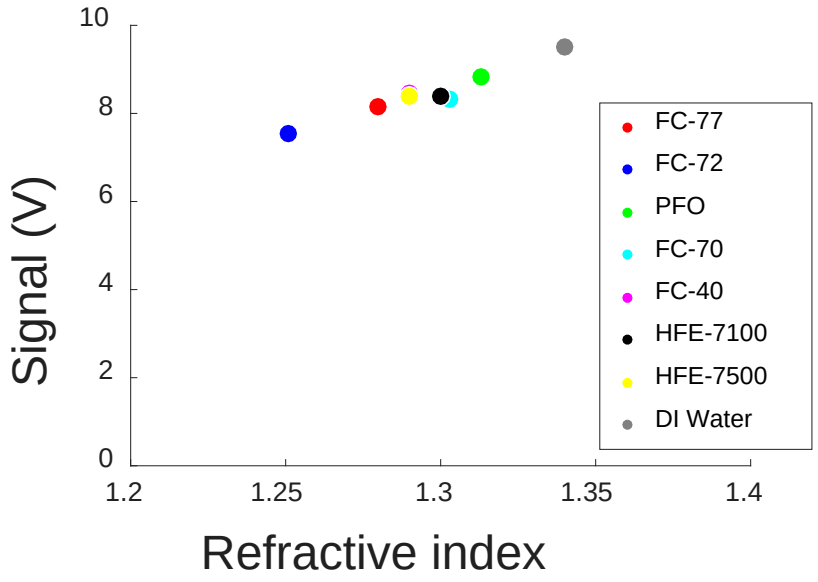

Fig S3. Ascribing the invariant signal monitored by the photodiode detectors to the oil phase (marked with black arrows on the left of all panels in Fig. S2) may be initially puzzling, because it seems to suggest that the colourless oil absorbs with similar intensity as the evidently coloured WST-1 formazan dye. However, we interpret the output signal (in V) as a combination of the total amount of light directed towards the detection fiber for a given solvent (which depends mainly on how much it scatters light, including scatter as a function of its refractive index) as well as the amount of light absorbed. To probe the contribution of the refraction index to the output signal we measured the voltage signal for a number of pure carrier oil phases at constant LED power at 455 nm and plotted this signal as a function of their refraction index. The clear correlation between the refractive index of the phase used and the detected output intensity at constant LED power observed in this figure explains why HFE-7500 appears to have a different signal than de-ionized water, even though it does not absorb light at 455 nm. Using one oil phase, only the concentration of the chromophore is determining the signal output and the linearity of this signal against product concentration (Fig. 2c) suggests that it is faithfully reflecting product absorbance (refraction being constant for the buffer used).

.

A

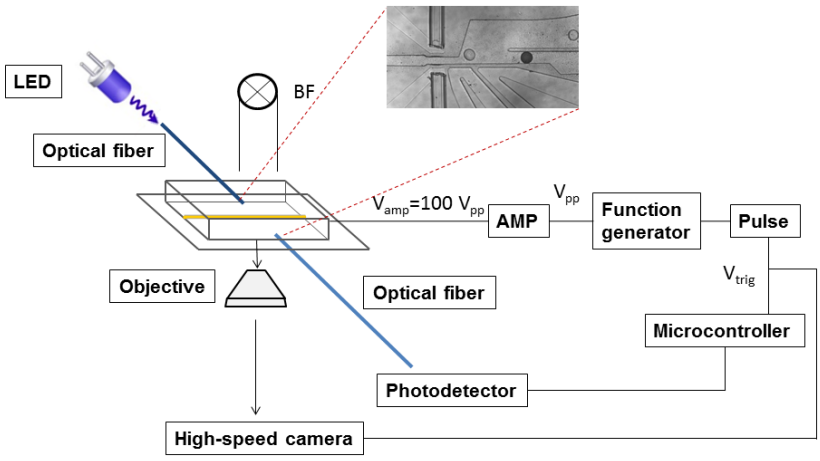

B

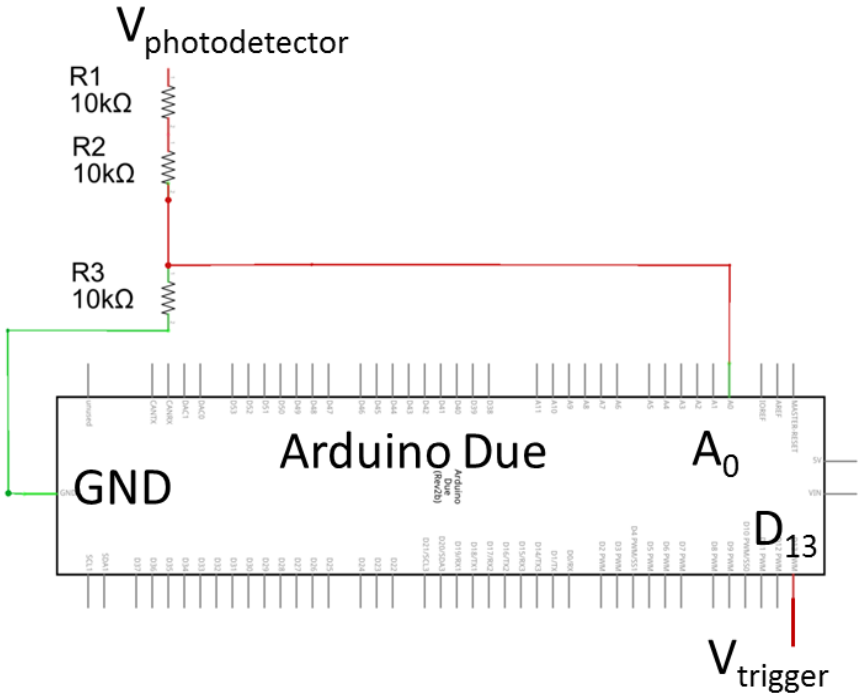

Fig. S4 Schematic of the AADS setup: the measurement of droplet transmittance is performed *via* the voltage measured by the photodetector. **A.** An Arduino Due microcontroller converts the analog voltage to a digital signal that can be used to generate a trigger signal. This signal will activate a 5 V pulse of typical width 5 ms which in turn triggers a function generator generating a 10 kHz square wave of amplitude 600 $V_{pp.}$ **B.** Wiring of the Arduino Due: the input signal from the

photodetector is divided 3 fold by resistors (to match the maximum voltage tolerable for the microcontroller board, i.e. 3.3V), and connected to an analog input of the Arduino (A_0). The trigger signal is exported to a digital pin (D_{13}) that is connected to the pulse generator.

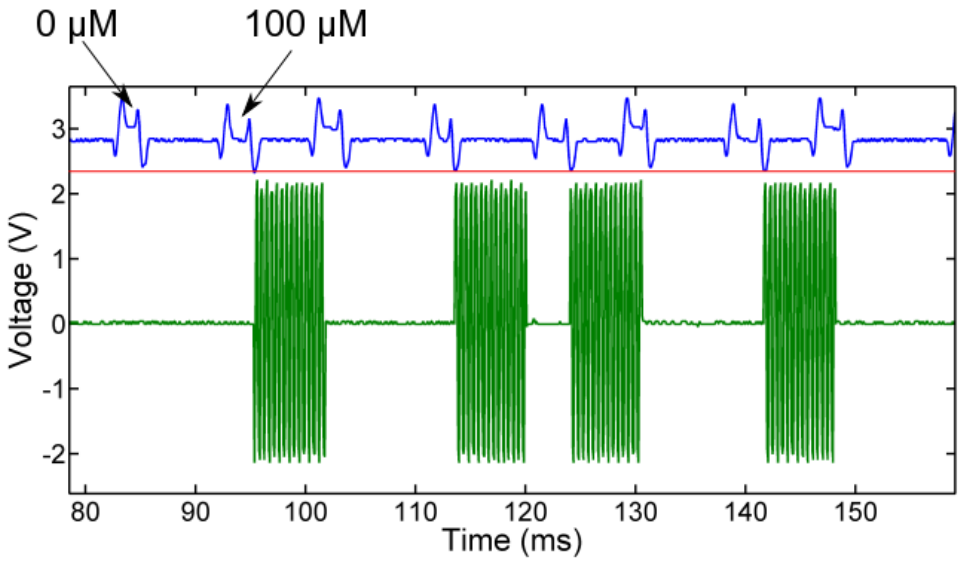

Fig. S5. Example of the raw signal from the photodetector measuring droplets containing 0 or 100 µM WST-1 formazan (in blue, divided by 3) and the corresponding AC wave used to trigger sorting before 100x amplification (in green). The sorting threshold is indicated by the red line. Only the droplets containing 100 µM WST-1 formazan result in a triggered signal.

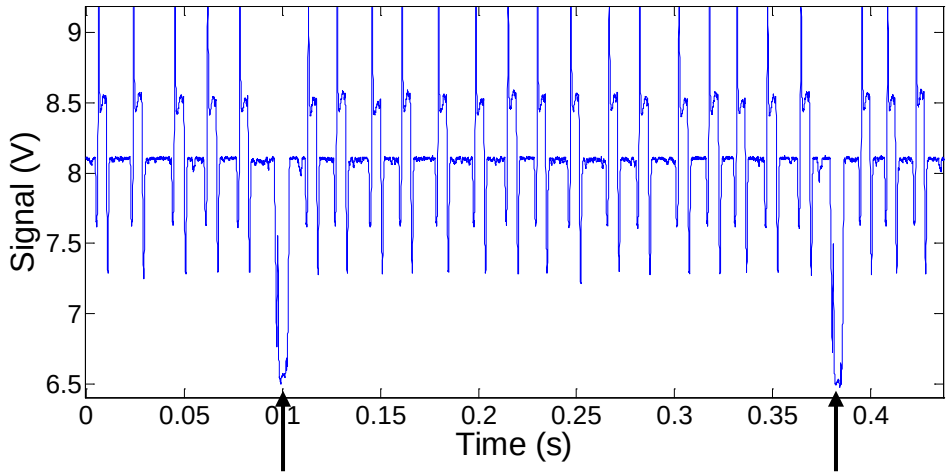

Fig. S6. Time-dependent single cell lysate in droplets for the reaction of wtPheDH. Example read-out after 4 hours incubation at an occupancy 0.1 cell/droplet. Black arrows indicate droplets containing a single-cell and where a reaction product is apparent**.**

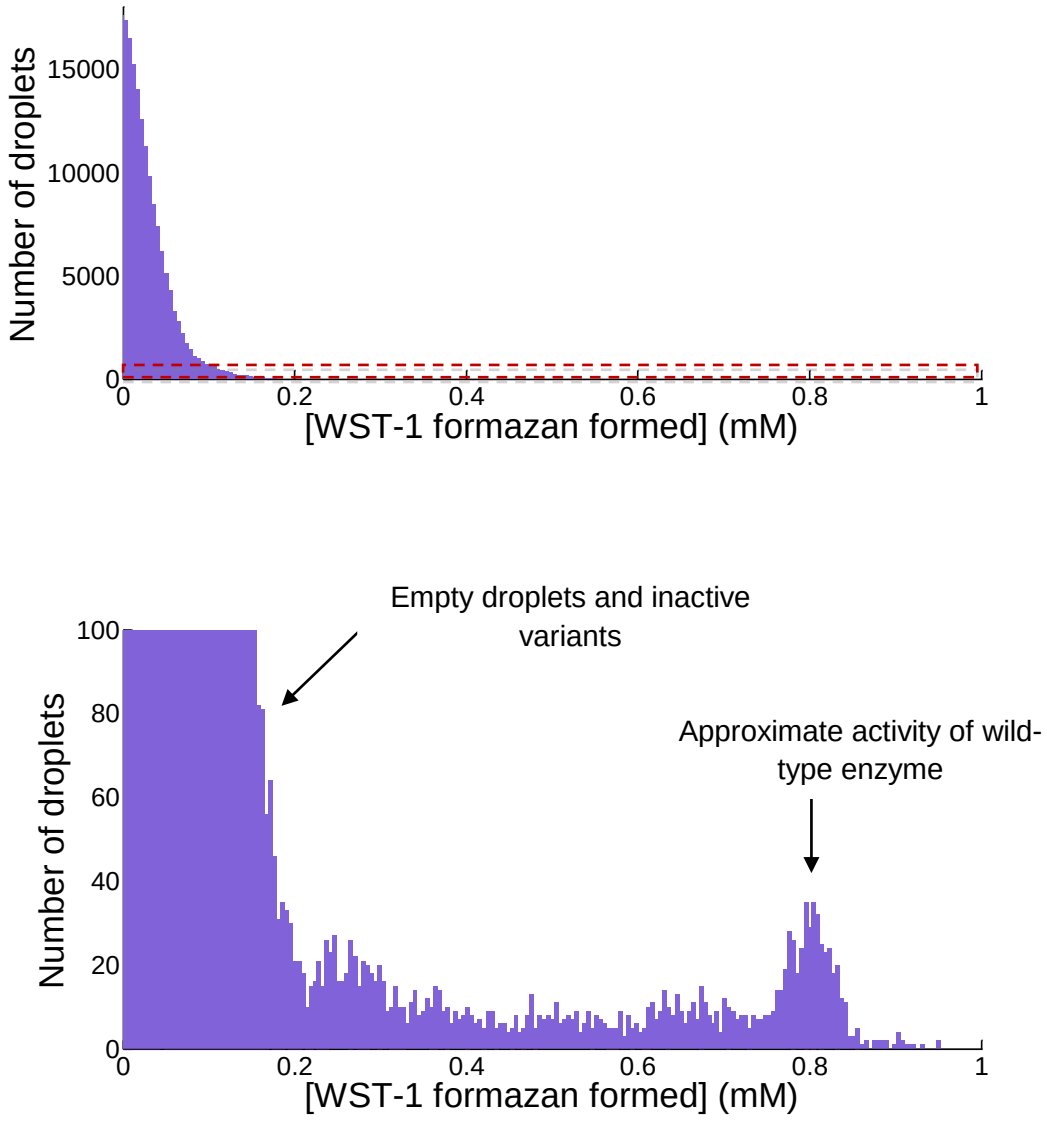

Fig. S7. Distribution function of a screening at [S] = 1 mM. A library generated by ep-PCR starting with PheDH$^{V26I/N122S/L193M/T339I}$ as the template was screened by AADS. A clear separation between active and inactive mutants is evident, suggesting that selections at relatively low substrate concentrations (1/10 of the substrate concentration used elsewhere in this paper) are feasible. For such selections, each of the bars inbetween the mutants with near wild-type and inactive could be chosen as a threshold (as in Fig. S7, right panel). *Conditions:* [glycine-KOH buffer] =100 mM, pH 10, 20 °C, saturating concentrations of [NAD^+] = 5 mM.

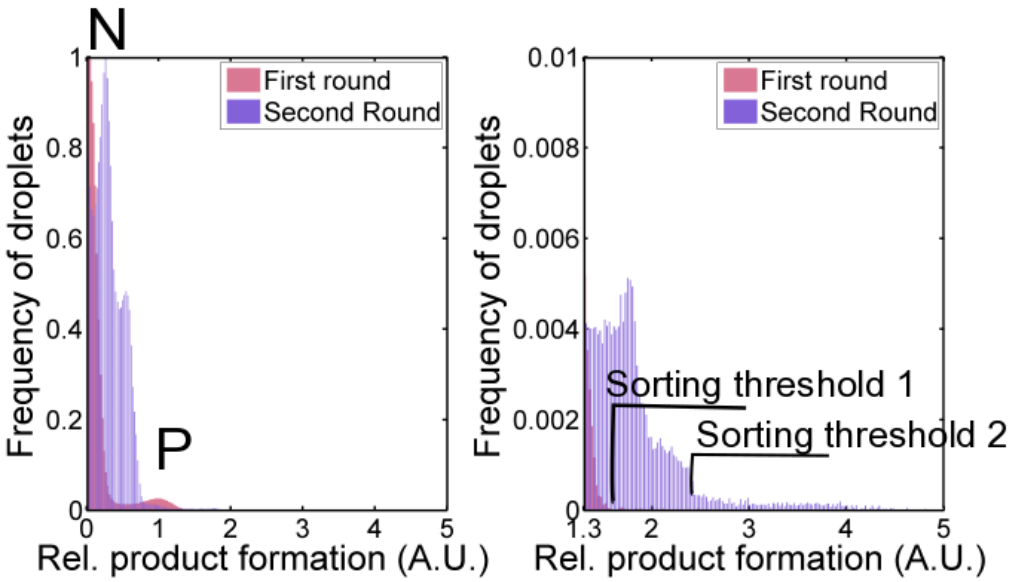

Fig. S8. Distribution function of **Lib0** (EpPCR: $5x10^5$ transformants encapsulated into 10^6 droplets) in pink and **Lib1** (shuffled variants: $1x10^5$ transformants encapsulated into 10^6 droplets) in purple; libraries screened for turnover of L-phenylalanine. The two histograms are derived from approximately 1 million droplets each. Poisson distribution dictates that most droplets (60% for the first histogram, and 90% for the second) do not contain a cell, so they form the left peak (N peak) together with droplets containing an inactive enzyme variant. The smaller peak on the right (P peak) and its perimeter corresponds to wtPheDH or variants with mutations that are silent or neutral. Low frequency peaks with higher product formation correspond to either multiple encapsulated cells (10% for the first histogram and 0.5% for the second, following Poisson statistics) or improved variants (0.01% after screening for each round). The arrows represent the sorting thresholds, corresponding to 1.5 and 2.5-fold improvements relative to the parental enzyme for the first and the second round of directed evolution, respectively.

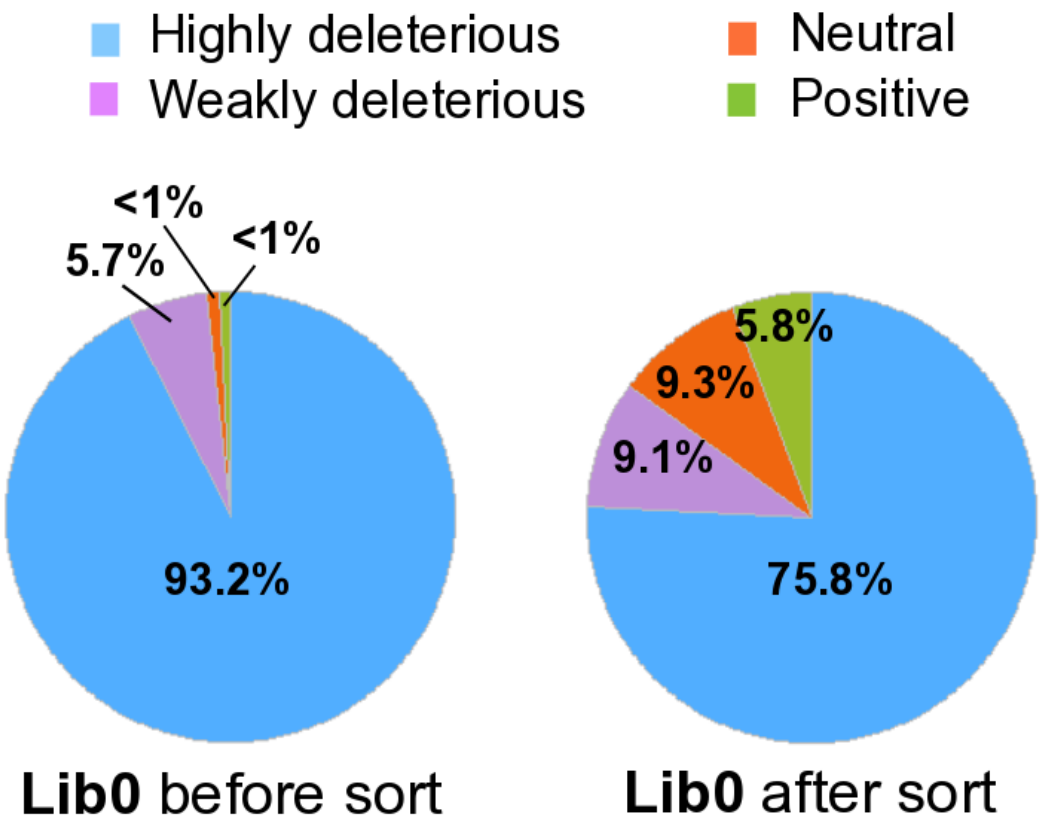

Fig. S9. Distribution functions of the dehydrogenase activities measured in cell lysate for **Lib0** before and after sorting with AADS. The activities are expressed relative to the activity of wtPheDH in cell lysate and assigned to four categories: (1) highly deleterious mutants (i.e. those with a >2-fold decrease in activity compared to wtPheDH), (2) weakly deleterious mutants (i.e. those with a 2-1.3 fold decrease), (3) neutral mutants (i.e. those ranging between a 1.3 fold decrease and a 1.3 fold increase), (4) positive mutant (i.e. those with a >1.3 fold increase). The increase in positives with increased activity and the decreasing fraction of mutants with deleterious mutations suggests that AADS selects for a catalytically relevant criterion (i.e. product formation), providing evidence for the utility of this new sorting module for directed evolution.

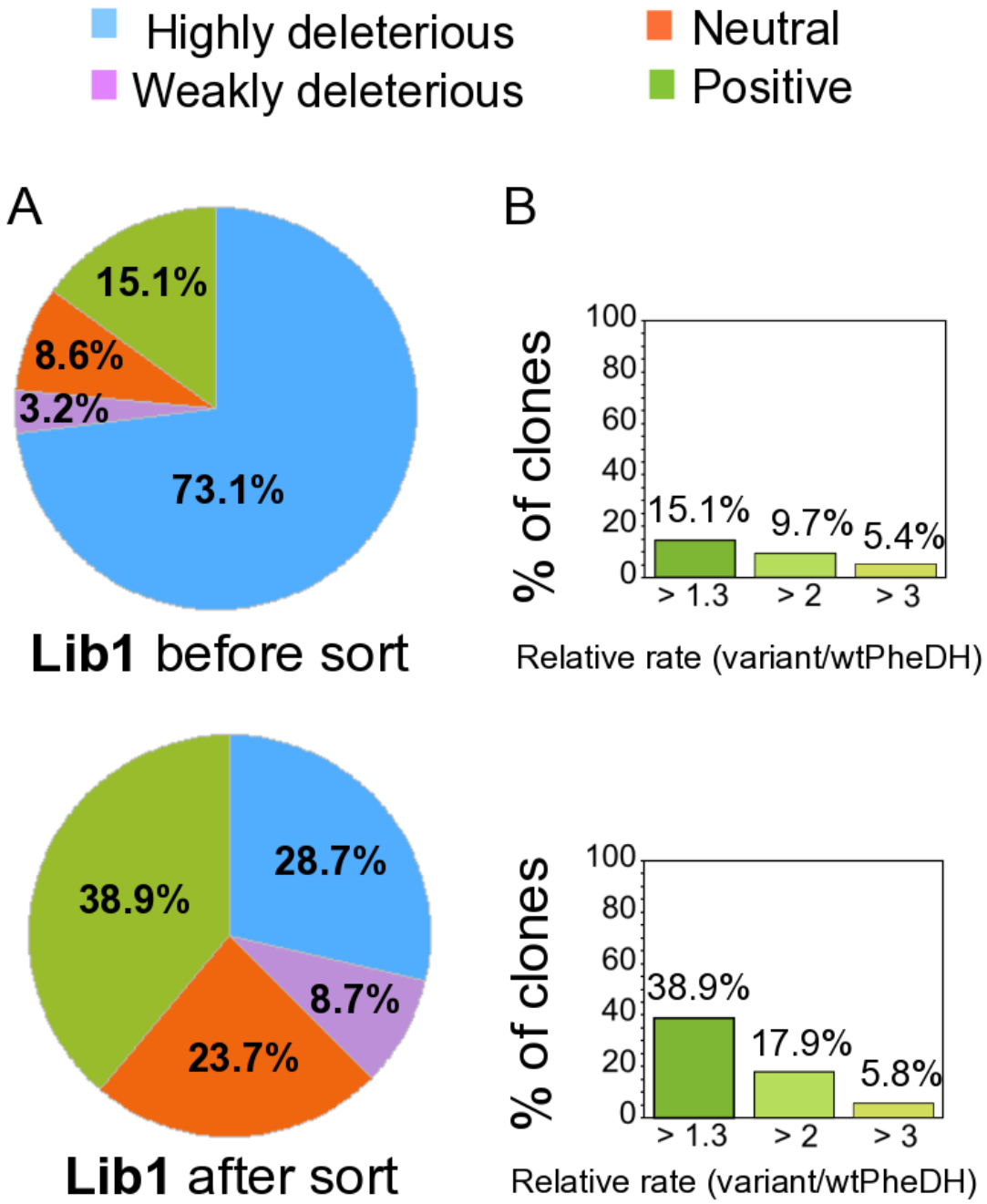

Fig. S10. Distribution functions of the dehydrogenase activities (measured as above) for **Lib1** before and after sorting with AADS. **(A)** The selected mutants (before and after sorting) cell lysate activities in 96 well plate are expressed relative to wtPheDH cell lysate activity, and clustered in four categories: the assignment to the four categories has been described in the caption to Figure S9. **(B)** Percentage of clones (from **Lib1**) with a relative activity *higher* than 1.3-, 2- and 3-fold compared to wtPheDH before and after sorting. The activity profile of the sorted population

showed that variants with >2-fold improved relative activity had been enriched by 2-fold during the sorting, reflecting the not very stringent screening regime.

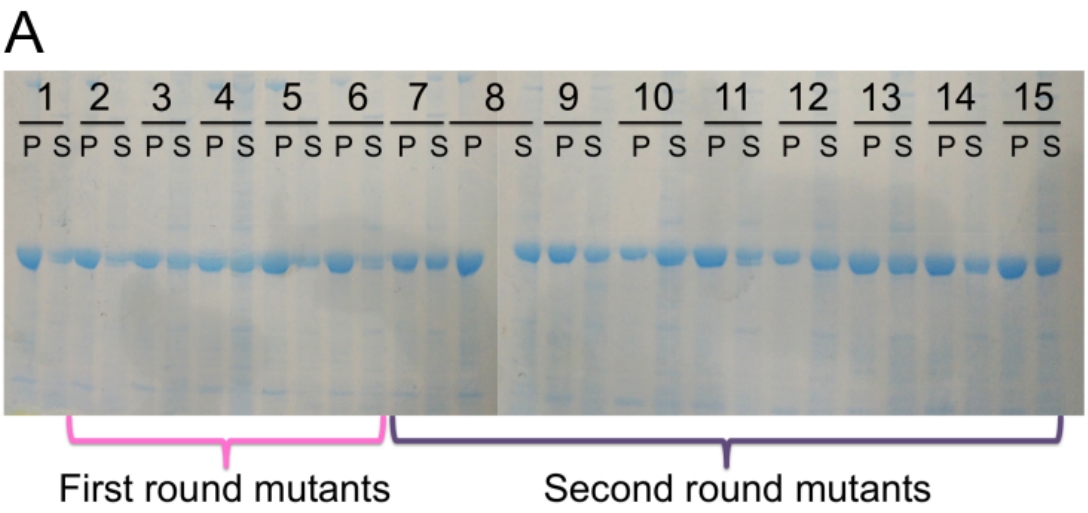

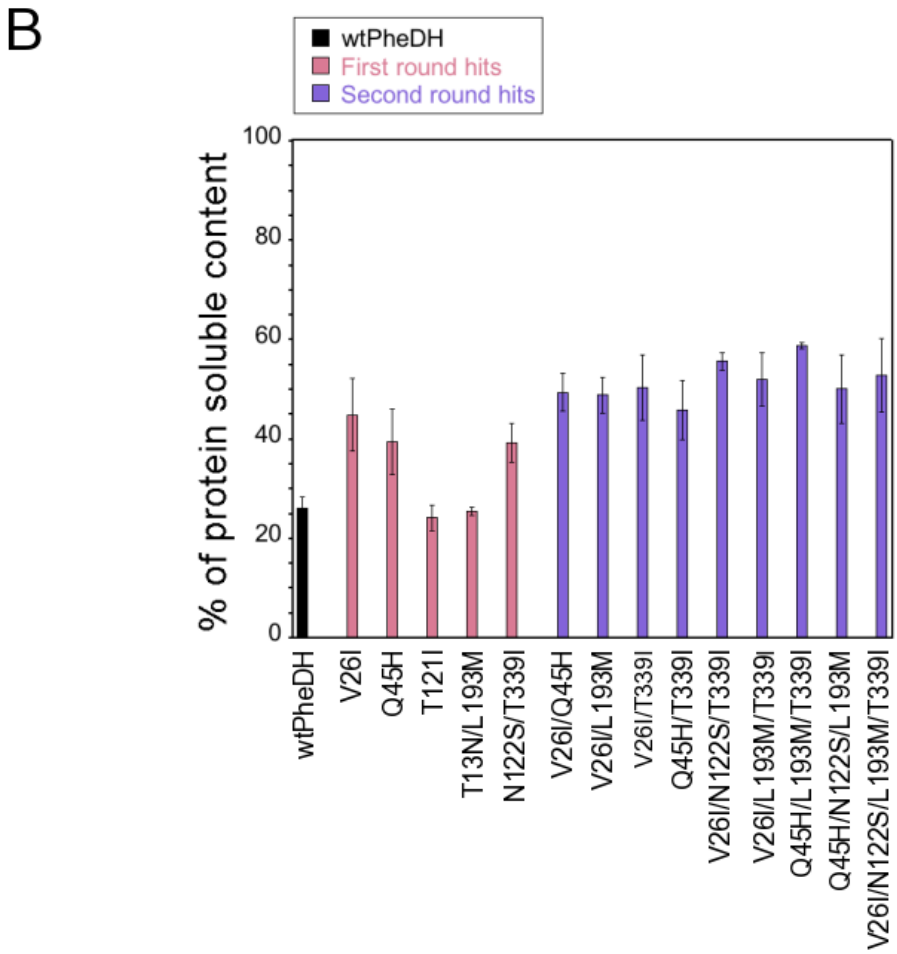

Fig. S11. Expression tests of the mutants selected by the first and second round of directed evolution. **(A)** Soluble expression levels of wtPheDH and selected variants. After protein expression, the soluble and insoluble fractions of cell lysates were analyzed by SDS-PAGE (12%). S: soluble fraction, P: pellet. Lane 1: wtPheDH, Lanes 2-6: first round mutants. Lane 2: clone T13N/L193M, 3: clone Q45H, 4: clone V26I, 5: clone N122S/T339I, 6: clone T121I, Lanes 7-15: second round mutants. Lane 7: clone V26I/L193M, 8: clone V26I/N122S/T339I, 9: clone V26I/N122S/L193M/T339I, 10: clone V26I/Q45H, 11: clone Q45H/N122S/L193M, 12: clone V26I/T339I, 13: Q45H/T339I, 14: clone Q45H/L193M/T339I, 15: clone V26I/L193M/T339I. **(B)** The percentage of enzyme in the soluble fraction was determined by the relative intensities of the supernatant and pellet bands. Error bars represent SEM of three independent measurements.

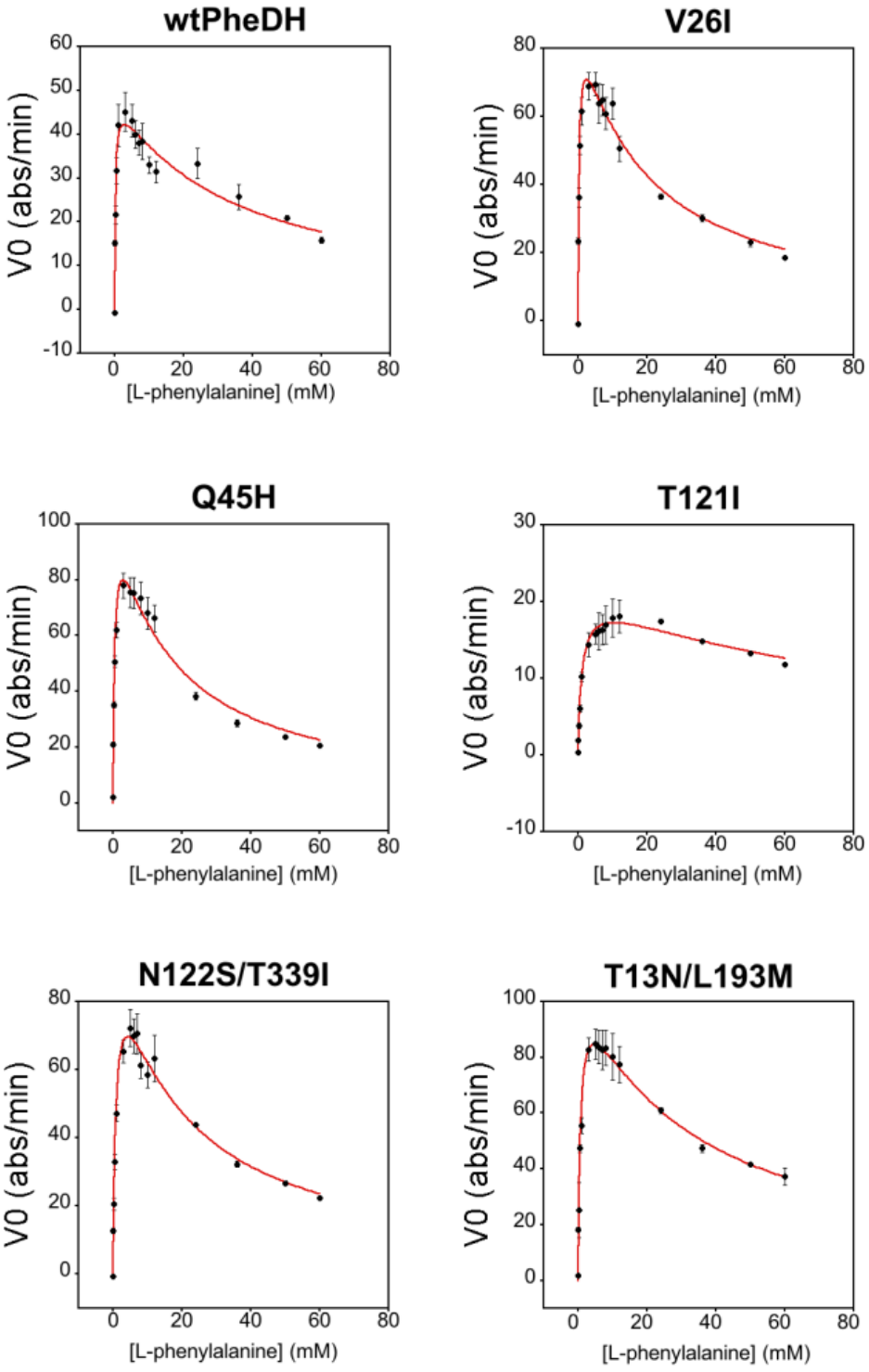

Fig. S12A. Michaelis Menten plots for first round mutants. *Conditions*: [glycine-KOH buffer] = 100 mM, pH 10, 20 °C, saturating concentrations of [NAD^+] = 5 mM.

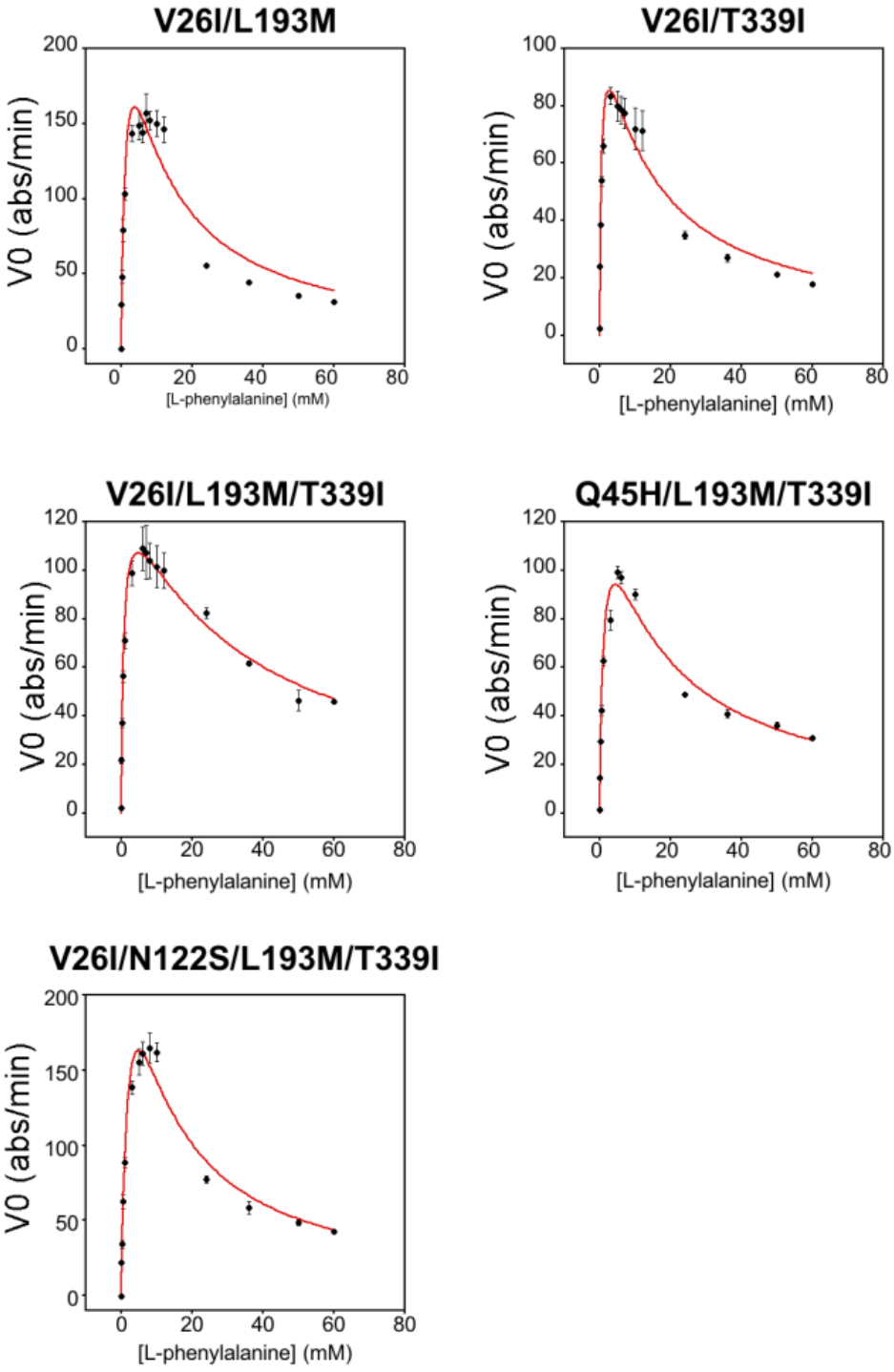

Fig. S12B. Michaelis Menten plots for second round mutants. *Conditions*: [glycine-KOH buffer] 100 mM, pH 10, 20 °C, saturating concentrations of [NAD^+]= 5 mM.

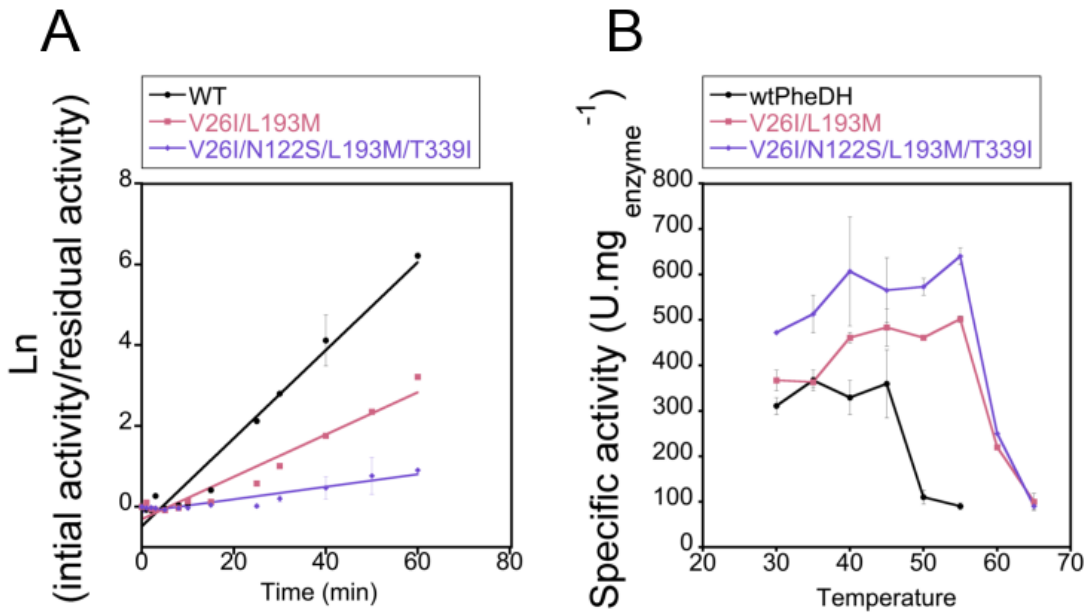

Fig. S13. (A) Thermal stability of wtPheDH and variants V26I/L193M and V26I/N122S/L193M/T339I at 50°C. wtPheDH and its variants were incubated at 50 °C, and samples were removed at regular time intervals and assayed for NADH production at 20 °C. **(B)** Temperature dependency of wild-type and variants V26I/L193M and V26I/N122S/L193M/T339I. Specific activities were measured over a range of temperatures from 30 °C to 65 °C in [glycine-KOH buffer] = 100 mM, pH 10, with 10 mM [L-Phe] and 5 mM [NAD^+].

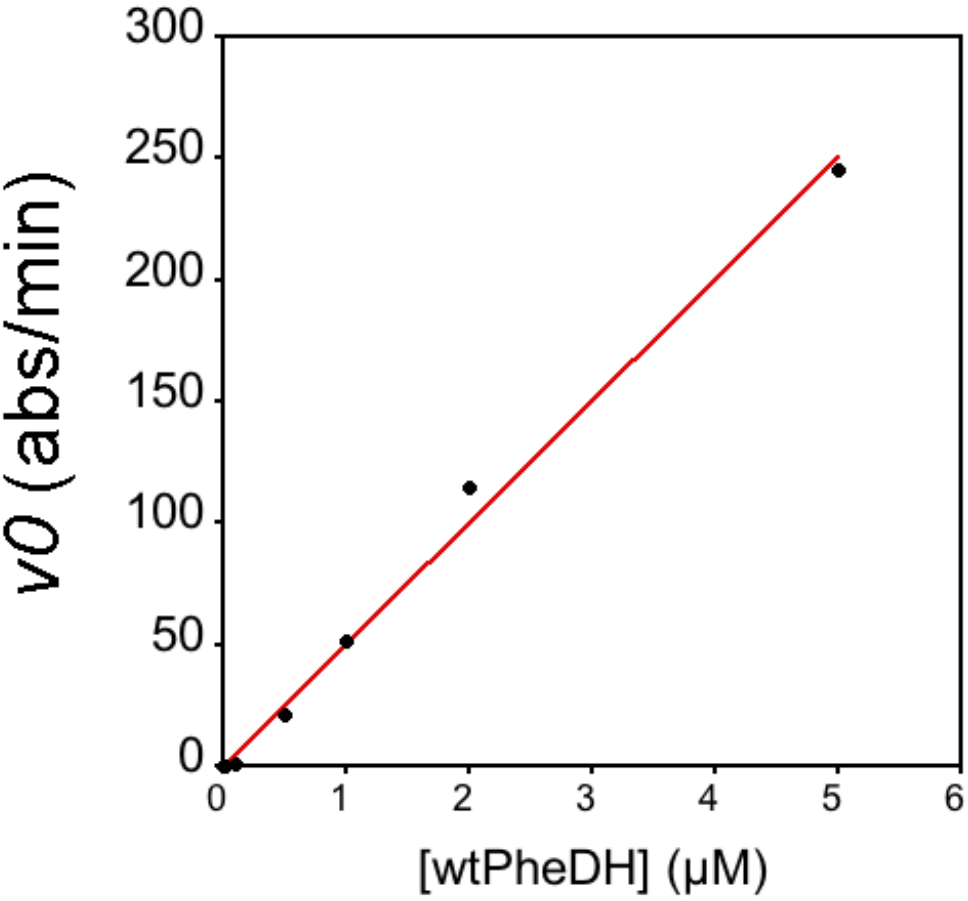

Fig. S14. Correlation of enzyme initial rates v_0 (wtPheDH) with enzyme concentration (measured with the spectrophotometer at 340 nM with [L-Phe] = 10 mM and [NAD^+] = 1 mM; [glycine-KOH buffer] = 100 mM, pH 10, T = 20 °C).

Table S1. Calculation of the number of enzyme molecules produced per cell for wtPheDH.

Dilution of lysate	v_0 (abs/min)[a]	Quantity of pure enzyme (wtPheDH) (µM) [b]	Number of molecules/L[c]	Number of cells/L [d]	Number of molecules/ cell [e]
1/1000	2.88	0.48	2.9×10^{16}	5×10^{10}	5.8×10^{5}
1/100	55.33	1	6.6×10^{17}	5×10^{11}	1.3×10^{6}
1/10	222.47	4.4	2.7×10^{18}	5×10^{12}	5.3×10^{5}
				Average	8.1×10^{5}

[a] Spectrophotometrically determined v_0 of NADH production at 340 nm. [b] Determined based on the titration shown in Fig. S14. [c]Calculated: (quantity of pure enzyme (in µM)[b] * N_A (Avogadro constant))/10^6; [d]Measured: OD_{600}, [e]Calculated: Number of molecules/L[c] / Number of cells/L[d].

The detection limit of the sorter is [WST-1 formazan]=10 µM, which corresponds to 6.022×10^{18} molecules/L (=10 N_A x 10^{-6}= 10^{-5} N_A; with $N_A = 6.022 \times 10^{23}$ molecules). The volume of one droplet is 180 pL, which means that at least **1.08×10^9** molecules WST-1 formazan (=6.022×10^{18} molecules/L x 180 x 10^{-12} L) must be present in one droplet.
Therefore, 1.08×10^9 molecules WST-1 formazan need to be turned over by 8.1×10^5 enzyme molecules, which means that 1333 turnovers (=1.08×10^9 / 8.1×10^5) are necessary per enzyme molecule to generate 10 µM of product WST-1 formazan.

Table S2. Michaelis-Menten parameters of the purified mutants from first and second round screens. Initial rate data ([S]=[L-Phe]= 0-60 mM) was plotted against substrate concentrations and fit to an equation containing a term for substrate inhibition ($v = k_{cat}$ [S] / (K_M + [S] + ([S]^2 /K_i)). *Conditions*: [glycine-KOH buffer] =100 mM, pH 10, 20 °C, saturating concentrations of [NAD^+] = 5 mM. Measured in a plate reader (SpectraMax 190, Molecular Devices).

Mutant	K_M (mM)	k_{cat} (s^{-1})	K_i (mM)	k_{cat}/K_M (10^3 $M^{-1}s^{-1}$)	*% protein soluble contents*
Wt	0.23 ±0.043	16.4 ±2.2	34 ±5.8	71.4 ±3.7	29 ±2.1
First round					
V26I	0.32 ±0.04	24 ±3.6	18 ±2	75±7	52 ±7.3
Q45H	0.44 ±0.14	29.4 ±5	17 ±5	66.9±6.12	46 ±6.2
T13N/L193M	0.73 ±0.07	29.7 ±3.4	30 ±2.8	40.7±9.89	27 ±2.5
T121I	21 ±0.07	2.8 ±0.73	90 ±13	0.13±0.81	25 ±0.8
N122S/T339I	1 ±0.14	30 ±5.6	18 ±2.4	30.3±4.54	36 ±3.8
Second round					
V26I/L193M	1.5 ±0.57	40 ±4	9 ±3.4	26.7±6.45	46 ±3.8
V26I/N122S/ L193M/T339I	2.6 ±0.03	45 ±5.6	10 ±3.8	17.3±1.45	58 ±6.5
V26I/L193M/T339I	0.66 ±0.16	17 ±1.02	35.7 ±7.9	26.4±0.62	52 ±6.0
V26I/Q45H	0.24 ±0.0001	9.2 ±1.0	18.7 ±2.0	56.7±4.26	55 ±1.7
V26I/T339I	0.58 ±0.04	33 ±2.7	13 ±2.7	56.8±0.58	60 ±0.6
Q45H/T339I	0.39 ±0.00039	21.9 ±1.0	43 ±11.6	56.3±4.26	57±6.8
Q45H/L193M/T339I	1.7 ±0.53	23.3 ±1.2	13.1 ±3.8	13.7±6.45	60 ±7.4

Table S3. T_m of the mutants selected by the two rounds of evolution. Directed evolution increased the T_m by up to 12.4 °C. Conditions: [MOPS buffer] = 100 mM with NaCl 150 mM, pH 8, and [glycine-KOH buffer] = 100 mM pH 10, [enzyme] = 2 μM.

	T_m (°C)		**ΔT_m (°C)**	
	pH 8	**pH 10**	**pH 8**	**pH 10**
wtPheDH	54.6 (±0.059)	47 (±0.03)	-	-
	First round mutants			
V26I	55.2 (±0.053)	47 (±0.1)	0.6	0
Q45H	53.4 (±0.08)	43 (±0.54)	-1.2	-4
T13N/L193M	57.2 (±0.094)	49 (±1.9)	2.6	2
T121I	N.D	N.D	N.D	N.D
N122S/T339I	56.3 (±0.07)	48.8 (±0.15)	1.7	1.8
	Second round mutants			
V26I/L193M	61.7 (±0.66)	50.5 (±0.12)	7.1	3.5
V26I/N122S/L193M/T339I	67 (±2.56)	54.7 (±0.07)	12.4	7.7
V26I/L193M/T339I	55 (±0.3)	51 (±0.05)	0.4	4
V26I/Q45H	N.D	N.D	N.D	N.D
V26I/T339I	58 (±0.27)	48.4 (±0.1)	3.4	1.4
Q45H/T339I	55.6 (±0.085)	48 (±0.06)	1	1
Q45H/L193M/T339I	42.1 (±0.08)	51.7 (±0.11)	-12.5	4.7

Table S4. Half-life of inactivation for wtPheDH and mutants V26I/L193M and V26I/N122S/L193M/T339I at 50 °C. Directed evolution increased the half life of inactivation by up to 7.5-fold.

Mutant	Half-life (min)	Half-life increase (n-fold)
wtPheDH	6	-
V26I/L193M	13	2.2
V26I/N122S/L193M/T339I	45	7.5